Networks and Spatial Economics
https://doi.org/10.1007/s11067-026-09798-z

RESEARCH

A Capacity-Constrained Spatial Equilibrium Model for Electric Vehicle Community Charging on Local Street Networks

Yang Song[1] · Xianbiao Hu[2] · Peiheng Li[3] · Xuesong Zhou[4]

Received: 3 June 2026 / Accepted: 18 October 2026
© The Author(s) 2026

Abstract

Community charging places electric vehicle (EV) chargers in communal spaces such as shopping malls, public parking, and activity centers embedded in local street networks. It creates a spatial equilibrium problem with an access and coupling structure that corridor charging along freeways does not exhibit. Multiple origin–destination pairs and routes converge on the same community charger via overlapping local arterials, so charger waiting times depend on the aggregate inflow from many paths and a single hardware capacity simultaneously constrains feasible flow for many travelers. On the physical network, these features make the generalized link costs non-separable across the links feeding a shared station. We formulate community charging as a capacity-constrained spatial equilibrium with station-level capacity side constraints, and we show it is exactly a Beckmann program with arc-capacity side constraints on a station-expanded network, restricted to range- and access-feasible paths. The capacitated user-equilibrium theory therefore applies, while the community-charging structure lies in the admissible paths and in the queueing origin of the station cost and capacity. We prove the cross-link symmetry that certifies the potential on the physical network, characterize the KKT solution as a generalized user equilibrium with endogenous station prices, and establish uniqueness of equilibrium flows under strict convexity. To solve the program, we develop a primal–dual decomposition: an outer augmented-Lagrangian loop adjusts station-level shadow prices on capacity, and an inner column-generation loop solves parallelizable path-flow subproblems for each OD pair under the current prices. Numerical experiments on a toy network, the Sioux Falls network, and two real-world community-charging networks show that the proposed method consistently attains equilibrium (to the reported tolerances) and outperforms a path-based interaction-ignored algorithm and a link-based interaction-aware Frank–Wolfe algorithm in computational efficiency.

Extended author information available on the last page of the article

Keywords Electric vehicle · Community charging · Spatial equilibrium · Capacity-constrained traffic assignment · Augmented lagrangian · Column generation

1 Introduction

Community charging refers to the strategic placement of electric vehicle (EV) charging stations in communal spaces such as community centers, shopping malls, parks, and public parking facilities embedded in *local street networks* rather than along freeway corridors (Zahedi et al. 2022; Zhang et al. 2023; Velkovski et al. 2024; Zhang and Fan 2025). Following the terminology adopted by the U.S. Joint Office of Energy and Transportation (Cardinali et al. 2023), community charging is contrasted with freeway-based corridor charging: DC fast chargers spaced tens of kilometers apart along interstates serving long-distance trips. Community charging instead embeds charging into routine activity patterns: residents without off-street parking, urban delivery fleets, ride-hailing drivers, and shared-mobility vehicles replenish their batteries while shopping, working, or parking near home. Federal programs such as the National Electric Vehicle Infrastructure (NEVI) program and the Charging and Fueling Infrastructure (CFI) Discretionary Grant Program have committed substantial resources to expand precisely this kind of community-scale infrastructure (USDOT 2023b, a).

Despite this policy momentum, the network-economic models used to analyze EV charging have largely been built around corridor settings, where each charger can be uniquely associated with a single freeway node or link and queues are essentially decoupled across origin– destination (OD) pairs. Section 2 reviews this literature in detail. Two structural features of community charging, however, fall outside the scope of those models:

(F1) Many-To-One Flow–Service Coupling Community chargers can be installed by local businesses or parking operators anywhere within communal spaces, and flows from multiple OD pairs and routes converge on the same facility via different local arterials. Waiting time at a community charger therefore depends on *aggregate* inflow from many links, so the generalized cost on a given link is influenced not only by its own flow but also by flows on other links feeding the same station, a many-to-one mapping from path flows to station queues that is absent in corridor models. As Section 4.2 shows, this coupling is a modeling feature that admits an exact equivalent representation, a station-expanded network on which every cost is separable (Proposition 2), rather than a structural obstruction.

(F2) Shared Station Capacity as Hard Side Constraints Each community charger has a finite physical service capacity that bounds the aggregate arrival rate it can sustain; exceeding that bound triggers congestion that propagates back through the network. The same hardware capacity therefore simultaneously constrains feasible flow for every OD pair and route that uses the station, so shared capacity constraints cou-

ple flows across otherwise independent OD pairs and destroy the Cartesian-product structure of the classical traffic-assignment feasible set.

Together, (F1) and (F2) make community charging a *capacity-constrained spatial equilibrium problem* that the corridor literature does not address, but the two features play asymmetric roles. (F1) is representational: on the physical network it makes the generalized costs non-separable, and the station-expanded representation of Section 4.2 removes it. What no representation removes is (F2): the shared station capacities remain hard side constraints on the expanded network. The problem is therefore exactly a *side-constrained* Beckmann program with range- and access-restricted admissible paths, rather than a standard assignment. This surviving constraint structure is the core difficulty, and the algorithm of Section 5 addresses it by dualizing the capacity constraints. The community-charging structure lies in the admissible paths and in the queueing origin of the station cost and capacity, not in a new equilibrium class.

This paper develops a model and a primal–dual algorithm tailored to this spatial structure. Our contributions are:

1. **Equilibrium characterization and equivalence.** We formalize community charging as a network-flow problem in which OD-level routing decisions are linked through *shared station-level capacity constraints* and *aggregated waiting-time interactions*: unlike corridor models, where each OD pair sees an effectively independent set of charger queues, routing is jointly constrained across OD pairs by a finite number of station-capacity budgets. For this structure we define a capacity-constrained generalized user equilibrium (Definition 1) in which endogenous station prices ρ_e clear the shared capacities. We prove it equivalent to the KKT system of a generalized Beckmann program whose equilibrium link-flow vector $\boldsymbol{x}^*$ is unique under strict convexity (Theorems 1–2; path-flow uniqueness is not required). We further show that the program is exactly a side-constrained Beckmann program on a station-expanded network restricted to range- and access-feasible paths (Proposition 2), with the cross-link symmetry (Lemma 1) as the physical-network certificate of the potential.
2. **Primal–dual decomposition algorithm tailored to shared-charger side constraints.** We design a primal–dual decomposition that exploits constraint family (F2) directly: the station-capacity constraints are dualized via an augmented Lagrangian that maintains *one multiplier per charger* rather than one per OD pair or per route, and the program decomposes into (i) an outer step that updates these station-level shadow prices and (ii) an inner column-generation step whose subproblem reuses the shortest-feasible-path construction of Section 3 to generate OD-level paths under the current prices. The shadow prices act as economic coordination signals between network-level capacity scarcity and OD-level routing, and the resulting algorithm outperforms both a path-based interaction-ignored algorithm and a link-based interaction-aware Frank–Wolfe algorithm in time-to-tolerance on networks up to Chicago-Sketch scale (Section 6.3; note that the interaction-ignored baseline converges on FI/RD residuals but does not reach the true generalized UE under active capacity constraints, as shown in Section 6.2). The

augmented-Lagrangian outer loop follows the classical multiplier theory of Hestenes (1969); Powell (1969), and Bertsekas (2015); the charger-indexed multiplier structure and the shortest-feasible-path subproblem are specific to the community-charging setting (the closest existing schemes are the augmented Lagrangean dual method of Larsson and Patriksson and the column-generation procedure of Larsson, Patriksson, and Rydergren; the precise differences from them are identified in Section 2.4).

3. **Computational evidence on networks of increasing size.** Numerical experiments on a toy network, the Sioux Falls network, the Eastern Massachusetts network, and the Chicago Sketch network show how the equilibrium responds to changes in charging supply and demand and document the responses of total system travel cost and aggregate dwell time, including the active station capacity constraints and the corresponding station-level shadow prices in the toy case. The experiments corroborate the algorithm's solutions by comparison with an interaction-ignored path-based baseline (which fails to reach equilibrium under active capacity constraints) and demonstrate its computational advantage over a link-based interaction-aware Frank–Wolfe baseline.

Section 2 provides a structured literature review and positions the paper relative to existing corridor-charging and capacitated traffic-assignment work. Section 3 introduces the network setting, notation, the shortest-feasible-path construction, and the link-performance approximation that captures demand–service interactions in polynomial form. Section 4 formulates the capacity-constrained spatial equilibrium model and states its equilibrium and uniqueness results (detailed proofs are deferred to Appendix B). Section 5 presents the primal–dual decomposition algorithm. Section 6 reports computational experiments. Section 7 concludes.

2 Literature Review

We organize the EV charging-network literature along three conceptual layers: a *demand* layer (which flows need to charge, at which stations, and along which routes), a *service* layer (queueing and waiting time at chargers), and a *resource* layer (the physical roadway network and the charger hardware itself). This layered view sits naturally within the spatial-economics tradition of treating shared infrastructure as a source of congestion externalities and demand agglomeration on capacity-constrained facilities. We organize the review along three classes of EV-charging models that engage progressively more of these layers (Sections 2.1–2.3), then review the methodological literature on capacitated traffic assignment with side constraints that informs our algorithmic approach (Section 2.4), together with the neighboring literatures on shared-facility congestion and non-separable equilibrium (Section 2.5), and finally position the paper against these bodies of work (Section 2.6).

2.1 Distance-Constrained Models

Early EV charging models were distance-constrained traffic assignment or location problems that focus almost exclusively on the resource layer (Jiang et al. 2012). They ensure feasible routes remain within battery range without explicitly modeling charging opportunities or queueing delays. Variants extend the Wardropian equilibrium principle by adding distance penalties, and have been used to study mode choice between gasoline and electric vehicles (Jiang and Xie 2014) and joint destination–route–parking choices under mixed gasoline/EV flows (Jiang et al. 2014). The demand layer is exogenous and the service layer is largely absent.

2.2 Subpath-Based Corridor Charging Models

A second group of studies allows en-route recharging at fast-charging stations along major corridors. By decomposing a long path into a sequence of feasible subpaths connected through charging events (Xie and Jiang 2016; He et al. 2014; Wang et al. 2016), these models can represent relay charging and incorporate station queues and the resulting dwell times from the service layer. Extensions analyze the impact of charging infrastructure and electricity prices on destination/route choice (He et al. 2013), elastic travel demand under charger layout (Huang and Kockelman 2020), charging plans that mitigate driver fatigue (Chen et al. 2023), flow-dependent EV energy consumption (Liu and Song 2018), and battery swapping (Xu et al. 2017). In these models chargers are assumed to lie along main corridors and can be uniquely mapped to nearby nodes (Stephens-Romero et al. 2010; Cavadas et al. 2015; He et al. 2016) or links (Hodgson 1990; Wang and Lin 2009; Capar et al. 2013), so many-to-many interactions between local streets and community chargers are not represented.

2.3 Community Charging on Local Street Networks

A third class of studies (community charging in shopping malls, public parking, and activity centers embedded in local street networks) has emerged in the policy and energy-systems literature (Zahedi et al. 2022; Zhang et al. 2023; Velkovski et al. 2024; Zhang and Fan 2025), but the network-economic side of the problem has received almost no formal treatment. The top panel of Fig. 1 contrasts this class with the corridor setting: a community charger sits off the freeway at a local activity center and is reached from multiple OD pairs through overlapping local arterials. No prior study, to our knowledge, formalizes community charging as a side-constrained network equilibrium with a queue-derived, flow-dependent station service cost and shared station-level capacity; this paper fills that gap.

2.4 Capacitated Traffic Assignment with Side Constraints

Methodologically, our model is an instance of traffic assignment with side constraints. Two routes to finite capacity emerged early: folding capacities into the cost implicitly, via asymptotic link performance functions (Daganzo 1977a, b), and imposing explicit capacity constraints priced by multipliers. The second route was initiated in

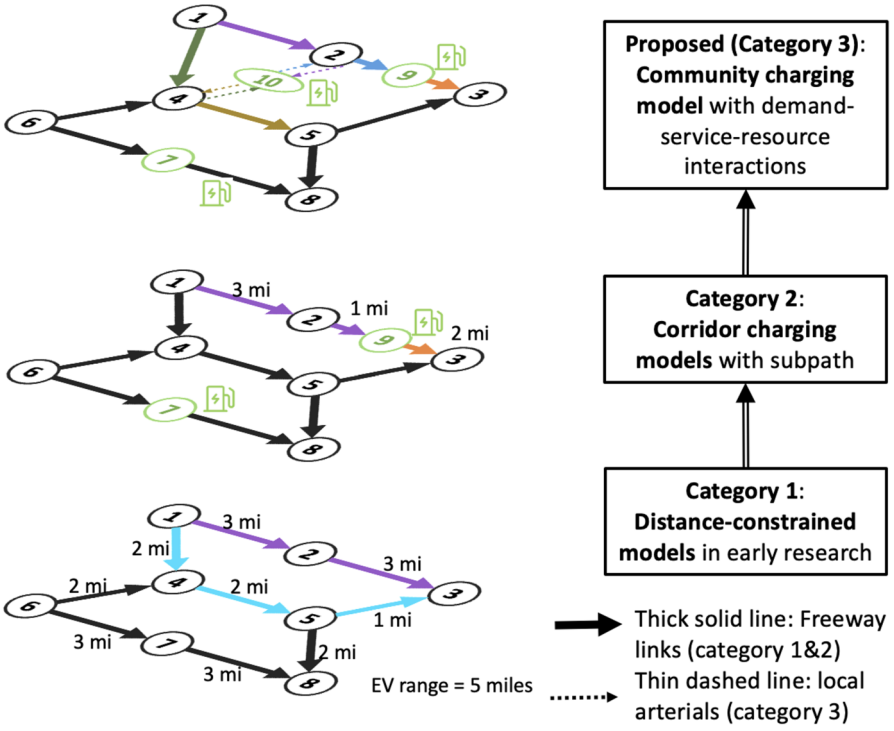


Fig. 1 Three categories of EV charging-network models on a common stylized network. Bottom: distance-constrained models. Middle: subpath-based corridor models with chargers on the freeway. Top (this paper): community charging, with a charger placed off the freeway at a local activity center and reached via overlapping local arterials

penalty form in an unpublished 1980 report by Hearn, as recounted by Larsson and Patriksson (1995), and developed systematically in the augmented Lagrangean dual algorithm of the same paper, the side-constrained equilibrium analysis of Larsson and Patriksson (1999), and the model and algorithm comparison of Nie et al. (2004). Ferrari (1997) reads the capacity multipliers as tolls; Shahpar et al. (2008) develop a dynamic penalty method; Meng et al. (2008) extend capacity constraints to stochastic user equilibrium. Capacity limits are typically dualized via Lagrange multipliers and an augmented penalty term in an augmented Lagrangian (ALM) framework (Feng et al. 2020). Frank–Wolfe and gradient-projection solvers underpin classical TAP (Sheffi 1985), with path-based gradient projection (Jayakrishnan et al. 1994) the standard path-space workhorse, and column generation has long been used to enumerate paths on demand, in the side-constrained setting by Larsson et al. (2004). More recent primal–dual decompositions for side-constrained TAP draw on the multiplier theory of Hestenes (1969), Powell (1969), and Bertsekas (2015), with distributed variants relying on parallel and distributed computation (Bertsekas and Tsitsiklis 2015).

A parallel strand asks what the capacity multipliers mean behaviorally. Yang and Yagar (1994) show that at saturated bottlenecks the multipliers are exactly the equilibrium queueing delays; Bell (1995) obtains the same reading in a stochastic user

equilibrium with explicit queues; Larsson and Patriksson (1999) analyze the delay and toll interpretations of side-constraint multipliers; Marcotte et al. (2004) instead treat hard capacities through strategic access probabilities. The pricing reading of the station price ρ_e adopted in Section 3.5 (a capacity-clearing access price, read as the implicit price of rationing where no charge is posted) inherits the toll-type interpretation of this tradition, with the queueing reading retained as its physical realization at saturated stations. In community charging, the priced resource is a shared off-network facility fed by several physical access links and OD pairs; on the expanded network of Section 4.2, it is a single constructed service arc.

Within the side-constrained assignment family, the closest existing schemes to the proposed ALM–column-generation algorithm of Section 5 are the augmented Lagrangean dual method of Larsson and Patriksson (1995), which dualizes the capacity side constraints, and the column-generation procedure of Larsson et al. (2004), which generates the path set on demand in the same side-constrained setting. Together they supply the dualization and path-generation halves that our scheme combines. Three ingredients are specific to community charging. First, the capacity constraints attach to the $|F|$ station service arcs of Section 4.2 rather than to pre-existing road links, so each dual ρ_e carries a facility-level reading. On the physical network it prices the joint inflow that several access links and OD pairs deliver to one station (F1), and by Proposition 2 it is, at the same time, the ordinary arc-capacity dual of that station's service arc. Second, the inner subproblem generates *range-feasible* paths under the station-access discipline of Section 3.2, a path family that link-capacitated schemes do not need. Third, the service cost w_e and the stability capacity $\alpha\mu_e$ of Eq. (13) are two faces of the same queueing model (Section 3.4), whereas in the link-capacitated literature the volume–delay function and the capacity bound are typically independent inputs.

2.5 Shared-Facility Congestion and Non-Separable Equilibrium

Community chargers belong to a family of shared, capacity-limited facilities embedded in networks, and the modeling questions they raise have close parallels in parking and transit. For parking, Bifulco (1993) evaluates parking policies within a stochastic equilibrium assignment; Lam et al. (2006) model time-dependent joint route and parking choices with explicit facility capacities; Boyles et al. (2015) analyze equilibrium search for scarce parking on a network. For transit, De Cea and Fernández (1993) formulate congested transit assignment, and Cominetti and Correa (2001) give a rigorous common-lines equilibrium under congestion. The game-theoretic root shared by these models is the congestion game of Rosenthal (1973), whose potential function underlies pure-strategy equilibria when players share congestible resources; the aggregation of our station term into a Beckmann-type potential (Section 4) is the continuous-flow counterpart. Conversely, the machinery developed here (the station-expanded representation, the queue-derived cost–capacity pair, and the station-indexed prices) applies beyond EV charging to off-network shared facilities whose service cost and capacity depend on aggregate throughput and whose access rules restrict the admissible paths; parking garages, curbside freight bays, and seaport berths are natural examples.

When such facilities are modeled directly on the physical network, the induced link costs are non-separable, which connects our formulation to the classical theory of equilibrium with link interactions. Dafermos (1971) introduced assignment with interacting links, Smith (1979) established existence, uniqueness, and stability of equilibria under monotonicity, and Dafermos (1980) gave the variational-inequality formulation that dispenses with integrability altogether. Lemma 1 places community charging at the tractable end of this spectrum: the cross-link interactions are symmetric, so a potential exists and the variational-inequality machinery is not needed; equivalently, the expanded representation of Section 4.2 renders the same program separable outright.

2.6 Positioning of this Paper

Figure 1 contrasts the three categories on a common stylized network: distance-constrained models (bottom panel) treat chargers only as range-extending nodes; subpath-based corridor models (middle panel) explicitly model station queues but assume chargers can be uniquely associated with single corridor nodes; community charging (top panel) places a charger off the freeway corridor at a local activity center that is reached from multiple OD pairs through overlapping local arterials, which is exactly the setting that induces (F1) and (F2). Table 1 summarizes how representative studies cover the demand–service–resource layers and which structural features they admit. The community-charging setting requires a model that explicitly captures (F1) the many-to-one flow–service coupling and (F2) shared station-level capacity, and that solves the resulting side-constrained spatial equilibrium efficiently. Among the prior studies tabulated in Table 1, none simultaneously models station-level shared capacity and a flow-dependent station service cost. Our model fills this gap: not with a new equilibrium class, but with a community-charging instantiation of side-constrained assignment (Section 4.2) whose admissible paths are range- and access-restricted.

3 Problem Setting and Preliminaries

3.1 Problem Overview

Before introducing the formal model, we briefly state the problem. A planner faces a road network that has been augmented with a known set of community chargers attached at communal-space nodes. OD demand is exogenous and all vehicles are EVs with finite battery range. The question is: *at user equilibrium, what is the joint distribution of route flows and charger arrivals when (i) generalized travel costs include a non-separable flow–service waiting time at each charger and (ii) each charger has a finite hardware capacity that simultaneously constrains all OD pairs that use it?* The model below addresses this question; charger siting and hardware sizing are not decision variables here.

The notation used throughout the paper is collected in Appendix A so it can be referenced from any section without searching the body text.

Table 1 Representative studies on EV charging networks and their coverage of the demand–service–resource layers.

Reference	Demand	Service	Resource	Stn. cap.	Stn.-coupled cost	Solution method
Jiang et al. (2012)	∘	–	•	–	–	path-constrained TAP
Jiang and Xie (2014)	•	–	•	–	–	mixed-mode UE
Jiang et al. (2014)	•	–	•	–	–	dest/route/parking choice
He et al. (2013)	∘	•	•	–	–	charger-deployment NLP
Xie and Jiang (2016)	∘	∘	•	–	–	relay-charging VI
He et al. (2014)	∘	•	•	–	–	subpath VI
Wang et al. (2016)	∘	•	•	–	–	trip-chain VI
Liu and Song (2018)	∘	•	•	–	–	flow-dep. consum. UE
Huang and Kockelman (2020)	•	•	•	–	–	elastic-demand UE
Chen et al. (2023)	•	•	•	–	–	resting-aware UE
Xu et al. (2017)	∘	•	•	–	–	swap + grade UE
Cavadas et al. (2015)	∘	–	•	–	–	MIP siting
He et al. (2016)	∘	–	•	–	–	siting w/ spatial factors
Hodgson (1990)	∘	–	•	–	–	flow-capturing location
Capar et al. (2013)	∘	–	•	–	–	arc cover–path cover
Feng et al. (2020)	∘	–	•	link-only	∘	ALM + GP
This paper	•	•	•	station	•	ALM + col. gen.

• = explicitly modeled; ∘ = implicit/exogenous; – = not modeled. Pure-siting/location papers without explicit demand or service modeling are included for completeness but participate only in the resource layer. "Stn.-coupled cost": the cost structure couples links through a shared station inflow; by Proposition 2 the coupling is representation-dependent (separable on the station-expanded network of Section 4.2)

We organize EV charging models along three conceptual layers (Fig. 2): a *demand* layer that captures which OD flows charge, at which stations, and along which routes; a *service* layer that characterizes charging at stations through a steady-state dwell relationship; and a *resource* layer comprising the physical roadway network and charger fleet. The two structural features (F1) and (F2) introduced in Section 1 arise precisely from the demand–service and service–resource interactions sketched in Fig. 2.

Scope: a Static, Steady-State Model The formulation developed below is static: OD demand q^{rs} is fixed, flows are time-invariant rates, and charging enters through the steady-state dwell function of Section 3.4 rather than through queue dynamics. In steady state, station inflow and outflow balance, so a link-based representation in which the aggregate inflow λ_e determines the station state is consistent. The model does not represent temporal demand variation, charging duration over time, queue evolution, or dynamic route and charging decisions; what a dynamic extension would require is discussed in Section 7.

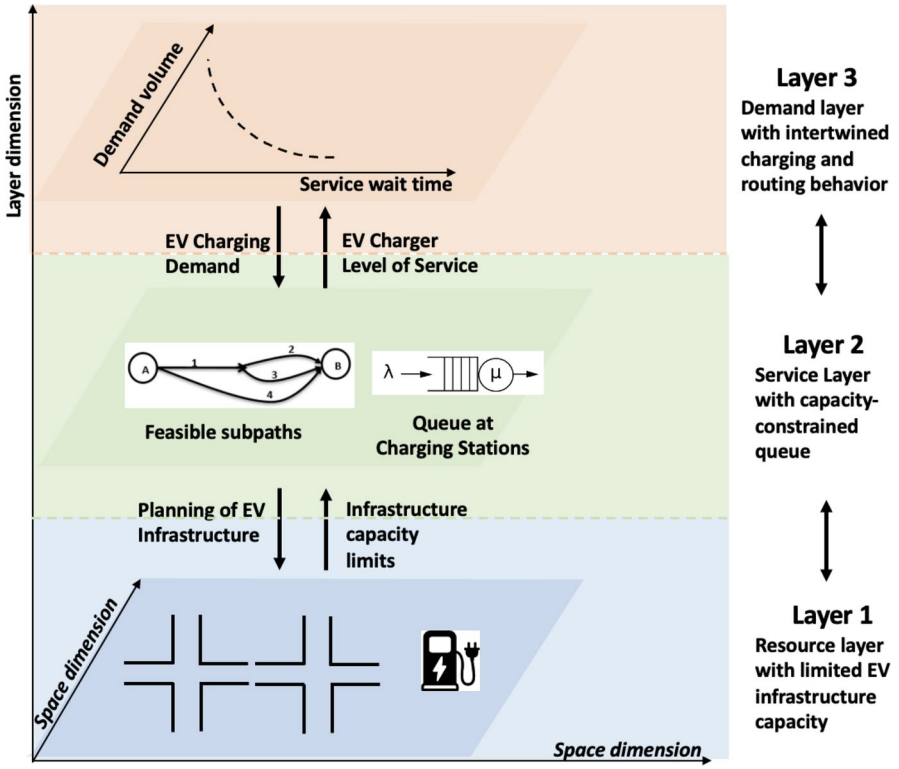


Fig. 2 Layered representation of the EV charging framework with three conceptual layers: demand (top), service (middle), and resource (bottom). The dashed inter-layer arrows on the left correspond to feature (F1) (many-to-one flow–service coupling); those on the right correspond to (F2) (shared station-level capacity). The sketch provides conceptual context and is more general than the model developed in this paper. Here the demand layer is instantiated statically (fixed, inelastic OD demand choosing routes and charging stations jointly), so the demand–wait-time curve sketched in the top layer is not part of the formulation. The service layer enters through the steady-state dwell function of Section 3.4. Temporal queue dynamics are outside the static scope (see the scope statement in Section 3.1 and the dynamic extension discussed in Section 7)

3.2 Network and Demand

EV drivers travel on a network $G = (V, E, F)$, where V is the node set, E is the link set, and F is the set of charging stations. Network expansion is performed first to integrate community chargers into the roadway network: nodes corresponding to charging infrastructure are added, together with the bidirectional arterial links that connect them to the surrounding street grid. This naturally partitions E into *connecting* (station-access) links E^c (the access links added between the street grid and the charger nodes, counted in both directions) and *non-connecting* links E^{nc}. Within E^c we further distinguish the *inbound* access links $E^{c,\text{in}} \subset E^c$, namely those terminating at a charger node. Only inbound flow contributes to station arrivals and incurs the station dwell time: the charger-inflow aggregation in Eq. (10) and the dwell term in Eq. (1) range over $E^{c,\text{in}}$, while outbound access links (and all non-connecting links) carry

only the road travel time. Because every access link is bidirectional, $|E^{c,\text{in}}| = |E^c|/2$; in the toy network of Fig. 3, $|E^c| = 8$ and $|E^{c,\text{in}}| = 4$.

Station-Access Convention A community charger is an *off-network* facility: it is reached from the street grid only through its access links and is not part of any through route. Five rules make the resulting movements precise. (i) *Same-access return*: a vehicle that enters charger e from access node v returns to the grid at the same node v; movements of the form $v \to e \to v'$ with $v' \neq v$ are excluded, so the facility cannot be used as a shortcut between grid nodes. Institutionally, this corresponds to an entrance–exit management rule (e.g., gated parking-style access at each entrance): users arriving from different access points do not traverse the facility, yet they share the same chargers and therefore contribute jointly to the aggregate station inflow λ_e and to the common waiting time. (ii) *Charging upon entry*: entering a charger node implies a charging event there; vehicles do not detour into a charging facility for any other purpose. (iii) *Charging optional at the strategy level*: a path in this model is a joint route–charging strategy; paths that visit no charger belong to the feasible set whenever their length permits (Section 3.3), so whether and where to charge is part of the route choice, not an imposed requirement. (iv) *At most one charging stop per station*: an itinerary charges at any given station at most once; returning to the same station for a second charging event is excluded. We state this as a modeling convention, not as a mathematical reduction: a charging event is a single completed service (Section 3.4), and a second charge at the same station lies outside the model's scope. Whenever a repeat visit would be *redundant* (its removal leaves the path feasible), the exclusion is also implied by strict cost domination, because the extra visit is a pure round trip that adds two access-link traversals and one dwell to an otherwise identical path. (v) *Link simplicity*: no directed link is traversed more than once. Under rule (i) a charging visit occupies the two *distinct* directed links (v, e) and (e, v), so every same-access round trip is permitted. Conventions (iv)–(v) make the binary incidences $\delta_a^{rs,p}$ and $\mathbb{1}_{[e \in p]}$ used in Sections 3.5 and 4 exact.

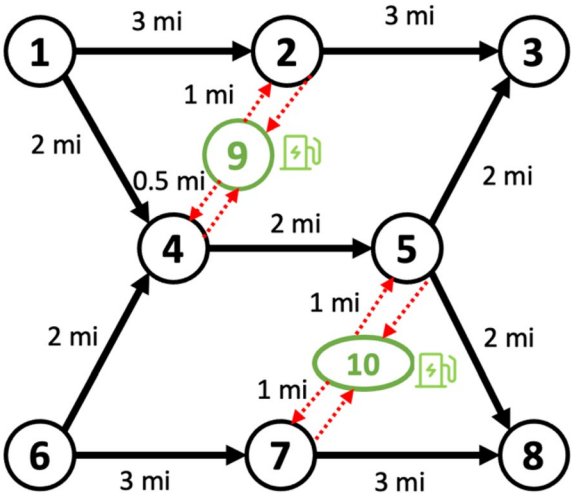


Fig. 3 Toy network with 8 original nodes (1–8), 9 corridor links (thick solid, with mileage labels), and two community chargers (nodes 9, 10, in green) attached via 4 bidirectional arterial links (thin red dashed). EV range $R = 5$ miles. OD demands: $q^{1,3} = 20$ and $q^{6,8} = 10$. Chargers are off-network facilities: each visit enters and leaves through the same access node (e.g., $2 \to 9 \to 2$), and through movements such as $2 \to 9 \to 4$ are excluded (Section 3.2)

Figure 3 illustrates the construction on a stylized toy network used throughout the paper. The base network has 8 nodes (1–8) and 9 corridor links. Two community chargers are added at nodes 9 and 10 via four bidirectional arterial links (2–9, 4–9, 5–10, 7–10). Two OD pairs are present: (1, 3) with demand $q^{1,3} = 20$ and (6, 8) with demand $q^{6,8} = 10$. Battery range is fixed at $R = 5$ miles. Under this setting, the OD pair (1, 3) has four feasible paths once range and the chargers are accounted for, three of which charge at most once and form its feasible path set under the one-stop scope of Section 3.3.

3.3 Shortest Feasible Path Set

A *feasible path* is one that an EV can traverse without depleting its battery, with or without recharging en route. Formally, a *subpath* is a maximal sequence of consecutive links that starts either at the origin or at a charger and ends either at a charger or at the destination. A path is feasible if every subpath has length at most R and the path obeys the station-access conventions (i)–(v) of Section 3.2: charger e entered from access node v is left through v (the visit appears in the node sequence as $v \to e \to v$), each station is charged at most once, and no directed link is traversed more than once. For instance, in the toy network of Fig. 3, OD pair (1, 3) admits four feasible paths: $1-2-9-2-3$, $1-4-9-4-5-3$, $1-4-5-10-5-3$, and $1-4-9-4-5-10-5-3$, while $1-2-3$ and $1-4-5-3$ are infeasible because their lengths exceed the 5-mile range.

To control the path-set size that the column-generation step in Section 5.2 must search, we restrict attention to a *shortest feasible path set* $\widetilde{P}_{rs}$ for each OD pair, generated by Algorithm 1 in Appendix B.7. The construction is justified by the following observation.

Proposition 1 *EV drivers prefer to minimize the number of charging events on their trips, as long as the resulting path remains feasible.*

See Appendix B.2 for the proof. By Proposition 1, paths that visit redundant chargers (e.g., $1-4-9-4-5-10-5-3$, which recharges at both 9 and 10) are dominated and can be discarded during path generation.

Scope: at most one Charging Stop Per Itinerary Throughout this paper, the feasible path sets P_{rs} are further restricted to itineraries with at most one charging stop: a path is either range-feasible without charging or charges exactly once. This restriction is stronger than convention (iv) of Section 3.2, which only excludes a second stop at the *same* station, and it is a modeling choice: community charging serves trips on a local street network, and at current EV ranges (a median of 283 miles per charge for model-year 2024 vehicles in the United States, U.S. Department of Energy (2024)) a day's travel, let alone a single trip, is typically within one battery charge (Needell et al. 2016), so that a trip needs at most one charging stop en route; moreover, in all experiments of Section 6 the range and the charger deployment are set so that every OD pair admits at least one feasible itinerary with at most one stop. Under the restriction, the feasible set of OD pair (1, 3) in Fig. 3 consists of the first three paths listed

above; the fourth, which charges twice, is in any case dominated by Proposition 1. Itineraries with two or more charging stops, which arise on long trips such as travel across several states, are discussed as an extension in Section 7.

Algorithm 1 is a heuristic generator: it builds $\widetilde{P}_{rs}$ from the k shortest paths of the base network and repairs a range violation by inserting a single charging stop, trying every station accessible from the path (Appendix B.7), so $\widetilde{P}_{rs}$ need not contain every feasible path: an itinerary whose road portion is not among the k shortest road paths is not generated. The consequences for the algorithmic guarantees are stated in Section 5.3, and a comparison against full enumeration of feasible paths on the toy network is reported in Section 6.2.

3.4 Interaction-Aware Link Performance Function

For an inbound access link $a \in E^{c,\text{in}}$ terminating at charger $e \in F$, the generalized link cost has two components: a road-traffic travel-time $t_a^{\text{road}}(x_a)$ that depends on its own flow x_a, and a dwell time $w_e(\lambda_e)$ at the charger that depends on the *aggregate* inflow λ_e from *all* links terminating at e:

$$t_a(x_a, \bar{x}_a^e) \;=\; t_a^{\text{road}}(x_a) \;+\; w_e(x_a + \bar{x}_a^e), \qquad a \in E^{c,\text{in}}, \tag{1}$$

where $\bar{x}_a^e = \sum_{a' \in E^{c,\text{in}},\, a' \neq a} \delta_{a'e}\, x_{a'}$ is the inflow to charger e from incoming links other than a. For all other links (outbound access links and non-connecting links), the dwell-time term is absent and $t_a(x_a) = t_a^{\text{road}}(x_a)$.

The road component $t_a^{\text{road}}(\cdot)$ is modeled by the Bureau of Public Roads (BPR) function (Bureau of Public Roads 1964):

$$t_a^{\text{road}}(x_a) \;=\; t_a^0\left[1 + \alpha_{\text{BPR}}\left(\frac{x_a}{C_a}\right)^{\beta_{\text{BPR}}}\right], \tag{2}$$

with free-flow time t_a^0, link capacity C_a, and standard parameters $\alpha_{\text{BPR}} = 0.15$, $\beta_{\text{BPR}} = 4$.

Polynomial Dwell-Time Function Two parameters describe the service at station e: the base (uncongested) service time w_e^0, the time a vehicle spends at a station it finds empty, in time units; and the service rate μ_e, the maximum number of vehicles the station can serve per unit time, in vehicles per time unit. They are independent parameters, and their product is the number of parallel servers (charging points) at the station, $c_e = w_e^0\,\mu_e$: a station with c_e identical servers, each occupied by one vehicle for w_e^0, serves at most c_e/w_e^0 vehicles per unit time. The reciprocal relation $w_e^0 = 1/\mu_e$ holds only for a single-server station, $c_e = 1$. For such a station, modeling the charger as an $M/M/1$ queue gives the closed-form dwell time $w_e(\lambda_e) = (\mu_e - \lambda_e)^{-1}$ (Little 1961), which has a singularity at $\lambda_e \to \mu_e$ and is numerically unstable in iterative solvers. Following (Zhou et al. 2022), we approximate it by a second-order polynomial volume–delay function obtained by Taylor expanding w_e at $\lambda_e = 0$, written with the base service time explicit:

$$w_e(\lambda_e) \;=\; w_e^0\Big(1+\frac{\lambda_e}{\mu_e}+\frac{\lambda_e^2}{\mu_e^2}\Big), \qquad e\in F. \tag{3}$$

For $c_e = 1$, (3) is the Taylor expansion of $(\mu_e - \lambda_e)^{-1}$ truncated after the second order. For $c_e > 1$ we retain the same function, now read as a station-side volume–delay function of the utilization λ_e/μ_e: it equals the base service time at zero inflow, increases and is convex in the inflow, and remains finite at capacity, in the same spirit as the BPR function on road links. It keeps the queueing motivation of the single-server case but is not a truncation of the exact multi-server delay, whose form depends on c_e and not only on the utilization; the truncation-error analysis of Appendix B.1 accordingly refers to the single-server case only. In the experiments of Section 6, time is measured in units of the base service time, $w_e^0 = 1$ for every station, so that μ_e is expressed in vehicles per base service time and equals the number of parallel servers c_e at the station: the service rate $\mu_e = 30$ of Table 5 describes a station with 30 servers of unit service time, not a single server with service time 1/30. The dwell entries of Tables 3–6 equal $1 + \lambda_e/\mu_e + (\lambda_e/\mu_e)^2$. The polynomial form preserves the cross-link gradient information needed for primal–dual updates and ensures the generalized objective remains a convex polynomial in flows. The truncation error of the single-server approximation, and its interplay with the capacity constraint (13) and the station price of Section 3.5, are quantified in Appendix B.1. A detailed derivation is given in Appendix B.

3.5 Generalized user Equilibrium Condition

For OD pair $(r, s) \in W$ and feasible path $p \in P_{rs}$, the generalized path cost is the sum of the (now non-separable) generalized link costs along the path:

$$C_p^{rs} \;=\; \sum_{a\in E} \delta_a^{rs,p}\, t_a(x_a, \bar{x}_a^e), \tag{4}$$

where $\delta_a^{rs,p} = 1$ if link a lies on path p between r and s, and 0 otherwise.

A flow pattern $\boldsymbol{f} = \{f_p^{rs}\}$ is in equilibrium if no driver can unilaterally reduce her generalized cost by switching paths. When station capacity is scarce, however, physical path costs need not equalize across used paths: the enforced station capacities $\alpha\mu_e$, where $\alpha \in (0, 1]$ is the capacity safety factor defined formally in Eq. (13), ration access to the shared chargers, and the equilibrium must include, for every station, the price of that scarcity. We therefore define the equilibrium jointly over path flows and station-level prices. For station prices $\rho_e \geq 0$, $e \in F$, define the *augmented* generalized path cost

$$\widehat{C}_p^{rs}(\boldsymbol{\rho}) \;=\; C_p^{rs} \;+\; \sum_{e\in F} \mathbb{1}_{[e\in p]}\,\rho_e, \tag{5}$$

where $\mathbb{1}_{[e\in p]} = 1$ if and only if path p charges at station e; by convention (iv) of Section 3.2, a path charges at each station at most once, so the binary indicator equals the number of charging events of p at e.

Definition 1 (Capacity-constrained generalized user equilibrium). A pair $(\boldsymbol{f}, \boldsymbol{\rho})$ with $\boldsymbol{f}$ satisfying demand conservation (14), non-negativity (15) and the station-capacity constraints (13), and $\boldsymbol{\rho} \geq 0$, is a *capacity-constrained generalized user equilibrium* if for every OD pair $(r, s) \in W$ there exists a minimum augmented cost u^{rs} such that

$$f_p^{rs} > 0 \implies \widehat{C}_p^{rs}(\boldsymbol{\rho}) = u^{rs}, \quad \forall p \in P_{rs}, \tag{6}$$

$$f_p^{rs} = 0 \implies \widehat{C}_p^{rs}(\boldsymbol{\rho}) \geq u^{rs}, \quad \forall p \in P_{rs}, \tag{7}$$

and the prices are active only at saturated stations (complementary slackness):

$$\rho_e \left(\lambda_e - \alpha \mu_e\right) \; = \; 0, \qquad \forall e \in F. \tag{8}$$

When no station is saturated, condition (8) forces $\boldsymbol{\rho} = 0$ and Definition 1 reduces to the classical Wardrop conditions stated with the physical cost C_p^{rs}, extended to the non-separable cost setting induced by flow–service coupling at community chargers.

Interpretation of the Station Price The price ρ_e arises in Theorem 1 below as the KKT multiplier of the capacity constraint (13), and it admits two complementary readings as a component of travelers' perceived cost. *Pricing reading:* ρ_e is the opportunity cost of a scarce charging slot, the station-access charge that clears the shared capacity. An operator or reservation platform posting ρ_e time-equivalent units at each station makes Definition 1 a Wardrop equilibrium under capacity-clearing access charges. Where no charge is posted, the same solution is read as a *rationing equilibrium*: the capacities (13) ration access to the shared chargers, and ρ_e is the implicit price of that rationing, the standard toll-type interpretation of side-constraint multipliers in capacitated assignment (Larsson and Patriksson 1999; Ferrari 1997). *Queueing reading:* the rationing at a saturated station may be realized physically (queueing or admission control), and ρ_e is compatible with the equilibrium delay of that process, determined endogenously by the capacity-clearing condition (8) rather than by the dwell function (3). This is the classical reading of capacity multipliers as equilibrium queueing delays (Yang and Yagar 1994; Bell 1995). Both readings induce the same equilibrium flows; Section 6.2 illustrates them on the toy network. We adopt the pricing reading as primary in what follows (it identifies $\widehat{C}_p^{rs}(\boldsymbol{\rho})$ without any claim about unmodeled delay, and it matches the coordination-signal role the prices play in the algorithm of Section 5) and treat the queueing reading as its physical realization at saturated stations.

4 Capacity-Constrained Spatial Equilibrium Model

4.1 Optimization Formulation

We pose community charging as the following constrained convex optimization problem. The decision variables are the path flows $\boldsymbol{f} = \{f_p^{rs}\}_{(r,s)\in W,\, p\in P_{rs}}$; link flows

$\{x_a\}$ and charger inflows $\{\lambda_e\}$ are derived through the path-link and link-charger incidence relations (11)–(10).

Objective The generalized Beckmann potential consists of an integral over the road travel time and an aggregated integral over the charger dwell time:

$$\min_{\boldsymbol{f}\geq 0} Z(\boldsymbol{f}) = \underbrace{\sum_{a\in E}\int_0^{x_a} t_a^{\text{road}}(\omega)\,d\omega}_{\text{road travel time}} + \underbrace{\sum_{e\in F}\int_0^{\lambda_e} w_e(\omega)\,d\omega}_{\text{station dwell time}}. \tag{9}$$

The aggregation of the dwell-time term over each charger e rather than over each connecting link is justified by the symmetry property established in Lemma 1, which guarantees that (9) is a valid potential for the non-separable generalized costs in (1).

Definitional Constraints. The aggregate flow at each charger and the flow on each link are defined through:

$$\lambda_e = \sum_{a\in E^{c,\text{in}}} \delta_{ae}\, x_a, \quad \forall e \in F, \tag{10}$$

$$x_a = \sum_{(r,s)\in W}\sum_{p\in P_{rs}} \delta_a^{rs,p} f_p^{rs}, \quad \forall a \in E, \tag{11}$$

together with the link–charger incidence consistency requirement that each link is associated with at most one charger:

$$\sum_{e\in F} \delta_{ae} \leq 1, \quad \forall a \in E. \tag{12}$$

Capacity Side Constraint Each charger's aggregate inflow must not exceed a fraction $\alpha \in (0, 1]$ (a capacity safety factor) of its hardware service rate:

$$\lambda_e \leq \alpha\, \mu_e, \quad \forall e \in F. \tag{13}$$

A value $\alpha < 1$ holds the station strictly below saturation (a stability margin for the station queue); $\alpha = 1$ imposes the hardware service rate itself, which is the setting used in all experiments of Section 6. Constraint (13) couples flows across all OD pairs and routes that share a station and is the source of the primal–dual structure exploited in Section 5.

Demand and Non-Negativity Flow conservation and non-negativity of path flows close the formulation:

$$\sum_{p \in P_{rs}} f_p^{rs} = q^{rs}, \quad \forall (r,s) \in W, \tag{14}$$

$$f_p^{rs} \geq 0, \quad \forall (r,s) \in W,\ p \in P_{rs}. \tag{15}$$

Equations (9)–(15) together define the *capacity-constrained spatial equilibrium* program that we analyze in the remainder of this section.

4.2 Station-Expanded Representation: Equivalence to a Side-Constrained Assignment

The program of Section 4.1 admits a second, exactly equivalent representation in which every cost is a separable function of its own arc flow. Figure 4 illustrates the construction at one station of the toy network.

Construction of the Expanded Network The station-expanded network G' is obtained from G in three steps. Each charger node $e \in F$ is split into an *entry port* e^- and an *exit port* e^+. Each inbound access link $(v, e) \in E^{c,\text{in}}$ is redirected to (v, e^-) and each outbound access link (e, v) to (e^+, v); both keep their road cost t_a^{road} and their physical length. Finally, one *service arc* $a_e = (e^-, e^+)$ is added per station. The service arc carries the dwell cost $w_e(y_e)$ as a function of its own flow y_e, the capacity $y_e \leq \alpha\mu_e$ as an ordinary arc capacity, zero physical length, and the recharge event: the battery resets to full range on a_e. No other arc leaves e^-, so entering a station commits the vehicle to charging; rule (ii) of Section 3.2 becomes topological.

The Path Map Under conventions (i)–(v), every feasible path $p \in P_{rs}$ maps to a path $T(p)$ of G' by replacing each charging visit $v \to e \to v$ with $v \to e^- \to e^+ \to v$. The map T is a bijection onto its image $\Pi'_{rs} = T(P_{rs})$. It preserves every subpath length, because service arcs have zero length, and it carries the station inflow λ_e of Eq. (10) to the service-arc flow y_e; by convention (iv), each path traverses a_e at most once.

Proposition 2 *(Equivalence to a side-constrained Beckmann program). Under the station-access conventions of Section 3.2, the program (9)–(15) is identical, term by term, to the Beckmann program with arc-capacity side constraints on G' restricted to the admissible path families $\{\Pi'_{rs}\}$. Specifically, every original link keeps its road integral in (9); the station term of (9) becomes the separable arc integral of the service arc a_e over its own flow y_e; the station capacity (13) becomes the ordinary arc capacity $y_e \leq \alpha\mu_e$; and demand conservation (14) and non-negativity (15) are imposed over Π'_{rs}. Under T, feasible solutions correspond one to one, objective values coincide, and the two programs have the same KKT system; in particular, ρ_e is the arc-capacity dual of the service arc a_e.*

The proof, a direct verification, is given in Appendix B.3.

Consequences and Scope On G' the station term of (9) is a separable arc integral, so the validity of the potential is immediate in this representation. The symmetry certifi-

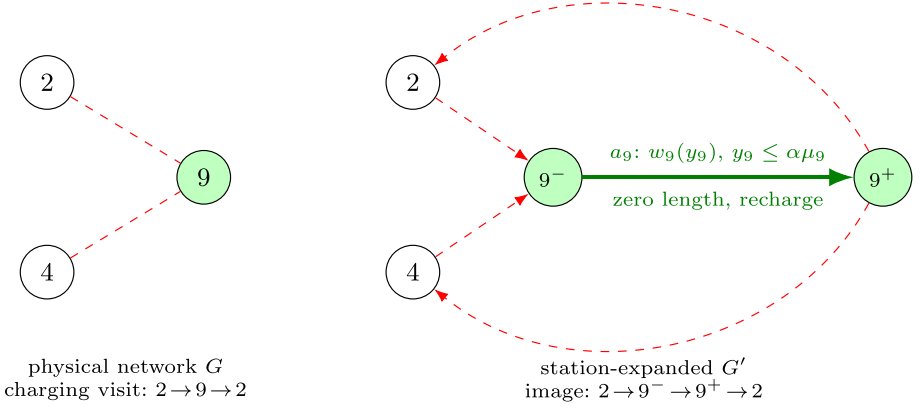


Fig. 4 The station-expanded representation at charger 9 of the toy network (Fig. 3). Left: on the physical network G, the charger is reached from access nodes 2 and 4 through bidirectional access links (dashed), and a charging visit takes the same-access return form $2 \to 9 \to 2$. Right: in G', node 9 splits into entry port 9^- and exit port 9^+, joined by the service arc a_9, which carries the dwell cost $w_9(y_9)$, the arc capacity $y_9 \le \alpha\mu_9$, zero physical length, and the recharge event. The access links are redirected to the ports, keeping their road costs and lengths. The only arc leaving 9^- is a_9, so entering a station implies charging (rule (ii)), and the visit maps to $2 \to 9^- \to 9^+ \to 2$

cate of Section 4.3 establishes the same fact directly on the physical network. Theorem 1 below is then the classical KKT–equilibrium equivalence of capacitated traffic assignment (Larsson and Patriksson 1999), applied verbatim to the restricted family Π'_{rs}, and ρ_e is the standard arc-capacity dual, read here as the capacity-clearing access price of the station (Section 3.5); dual variables need not be unique under degeneracy. The Proposition is a statement about the program, not about any algorithm. It provides no guarantee for the heuristic path-generation (pricing) step of Section 5, which operates on generated working sets $T(\widetilde{P}_{rs}) \subset \Pi'_{rs}$ (Section 5.3), and it does not imply that an off-the-shelf link-based capacitated solver applies unchanged, because the admissible family Π'_{rs} is range- and access-restricted rather than the full path set of G'. What is specific to community charging therefore lies in the admissible paths (range feasibility with recharge; the access discipline (i)–(v)) and in the queueing origin of the service cost w_e and the stability capacity $\alpha\mu_e$, not in the cost structure of the program.

4.3 Symmetry of Flow–Service Interactions

Lemma 1 *For any two inbound access links $a, b \in E^{c,\text{in}}$ converging at the same charger $e \in F$, the cross-link sensitivities of the generalized link travel time satisfy $\partial t_a/\partial x_b = \partial t_b/\partial x_a$.*

The proof, which uses the polynomial form of w_e, is given in Appendix B.4. This symmetry is the physical-network certificate that the cross-link interactions integrate into the generalized Beckmann potential (9). On the station-expanded network of Section 4.2 the same fact is immediate from separability; Lemma 1 verifies it directly on G, where the algorithm operates and the reported flows are defined.

4.4 Equivalence to user Equilibrium and Uniqueness

Theorem 1 *A feasible flow vector $\boldsymbol{f}^*$ is an optimal solution of the proposed model (Eqs. (9)–(15)) if and only if there exist station prices $\boldsymbol{\rho}^* \geq 0$ such that $(\boldsymbol{f}^*, \boldsymbol{\rho}^*)$ is a capacity-constrained generalized user equilibrium (Definition 1). The prices are the KKT multipliers of the capacity constraints (13).*

Theorem 2 *Under strict convexity of the generalized potential, the equilibrium link-flow vector $\boldsymbol{x}^*$ is unique.*

The proof of Theorem 1 matches the KKT system of the constrained program to the equilibrium conditions of Section 3.5 in both directions and is deferred to Appendix B.5; the convexity argument for Theorem 2 is deferred to Appendix B.6. The techniques follow standard traffic-assignment theory (Sheffi 1985); the problem-specific content of this section is the symmetry certificate (Lemma 1) together with the station-expanded equivalence (Proposition 2).

5 Primal–Dual Decomposition Algorithm

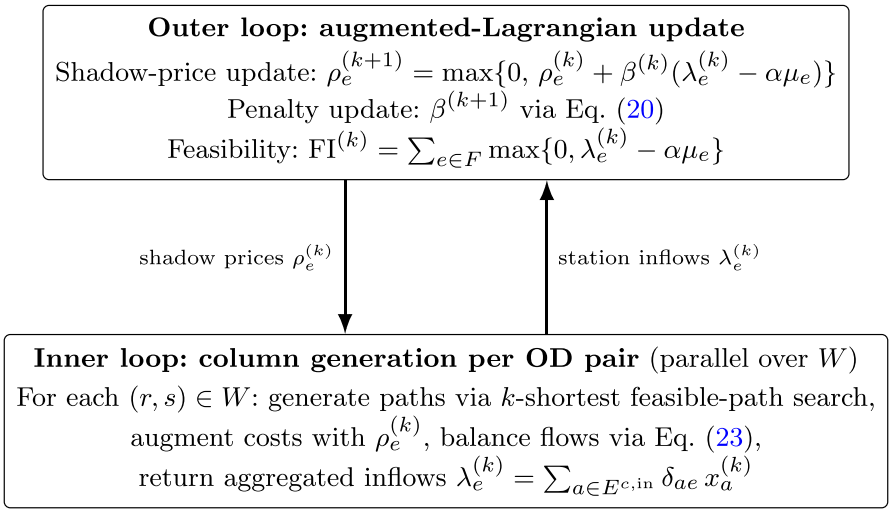
The capacity side constraint (13) couples flows across OD pairs and routes that share a station. To exploit decomposability of the remaining structure, we relax (13) via an augmented Lagrangian and design a two-level algorithm: an outer loop that updates station-level shadow prices $\boldsymbol{\rho}$ on capacity, and an inner loop that solves the resulting unconstrained generalized UE by column generation, with its per-OD-pair subproblems processed in parallel between cost synchronizations. The two loops act as a primal–dual decomposition (Fig. 5): the outer step sets prices that reflect network-wide capacity scarcity, and the inner step computes user responses to those prices in parallel across OD pairs. The shadow prices ρ_e admit a direct economic interpretation as the marginal value of additional capacity at station e.

5.1 Outer Loop: Augmented Lagrangian on Station Capacities

Introduce a non-negative slack $s_e \geq 0$ to convert the capacity inequality (13) into an equality:

$$\lambda_e + s_e - \alpha\,\mu_e \;=\; 0, \quad \forall e \in F. \tag{16}$$

The augmented Lagrangian of (9)–(15) with respect to (16) is



Terminate when $\mathrm{FI} \leq \gamma_1$ *and* relative duality difference $\mathrm{RD} \leq \gamma_2$.

Fig. 5 Primal–dual decomposition structure of the proposed augmented-Lagrangian column-generation (ALM–CG) algorithm. The outer loop dualizes the station capacity constraints (13) and updates one shadow price ρ_e per charger. The inner loop solves the resulting generalized UE per OD pair in parallel by column generation, then returns the aggregated station inflows λ_e to the outer loop. The algorithm terminates when both the flow infeasibility FI and the relative duality difference RD fall below their tolerances

$$L_\beta(\boldsymbol{f}, \boldsymbol{s}, \boldsymbol{\rho}) \;=\; Z(\boldsymbol{f}) \;+\; \sum_{e \in F} \rho_e (\lambda_e + s_e - \alpha \mu_e) \;+\; \frac{\beta}{2} \sum_{e \in F} (\lambda_e + s_e - \alpha \mu_e)^2 , \tag{17}$$

where $\rho_e \in \mathbb{R}$ is the station-level shadow price on capacity at e, and $\beta > 0$ is the penalty parameter. Minimizing (17) over $s_e \geq 0$ in closed form yields $s_e^* = \max\{0,\, \alpha\mu_e - \lambda_e - \rho_e/\beta\}$, and substituting back gives the slack-eliminated form

$$L_\beta(\boldsymbol{f}, \boldsymbol{\rho}) \;=\; Z(\boldsymbol{f}) \;+\; \frac{1}{2\beta} \sum_{e \in F} \Big[\max\{0,\, \rho_e + \beta(\lambda_e - \alpha\mu_e)\}^2 - \rho_e^2 \Big]. \tag{18}$$

For fixed $\boldsymbol{\rho}$ and β, problem (18) is an unconstrained generalized UE with shadow-price-augmented link costs, and is solved by the inner loop in Section 5.2.

Multiplier and Penalty Updates At outer iteration k, after the inner loop returns $\boldsymbol{f}^{(k)}$, the multipliers and penalty parameter are updated by

$$\rho_e^{(k+1)} \;=\; \max\Big\{ 0,\; \rho_e^{(k)} + \beta^{(k)} \Big(\lambda_e^{(k)} - \alpha \mu_e \Big) \Big\} , \quad \forall e \in F, \tag{19}$$

$$\beta^{(k+1)} \;=\; \begin{cases} \xi\, \beta^{(k)}, & \text{if } \mathrm{FI}^{(k)} > \iota \cdot \mathrm{FI}^{(k-1)}, \\ \beta^{(k)}, & \text{otherwise,} \end{cases} \tag{20}$$

where $\mathrm{FI}^{(k)} = \sum_{e \in F} \max\{0,\, \lambda_e^{(k)} - \alpha\mu_e\}$ is the flow-infeasibility measure, and $\xi > 1$ and $\iota \in (0, 1)$ are tuning constants (we use $\xi = 2$, $\iota = 0.25$ throughout). The multiplier update (19) follows the multiplier method of Hestenes (1969) and Powell (1969); the adaptive penalty rule (20) follows (Bertsekas (2015)).

Initialization We initialize multipliers and penalty as

$$\rho_e^{(0)} \;=\; \max\Big\{ 0,\; \beta^{(0)} \Big(\lambda_e^{(0)} - \alpha \mu_e \Big) \Big\} , \quad \beta^{(0)} \;=\; \frac{Z(\boldsymbol{f}^{(0)})}{\mathrm{FI}^{(0)} + \varepsilon}, \tag{21}$$

where $\boldsymbol{f}^{(0)}$ is an all-or-nothing assignment under free-flow costs and $\varepsilon > 0$ avoids division by zero.

5.2 Inner Loop: Column Generation per OD Pair

For fixed $\boldsymbol{\rho}$ and β, the inner problem (18) decouples by OD pair given the path flow vector restricted to its working set $\widetilde{P}_{rs} \subseteq P_{rs}$. For each OD pair (r, s) we (i) compute generalized link costs that combine (1) with the dualized capacity charge; (ii) generate new candidate paths via k-shortest feasible-path search on the physical network G (see Algorithm 1 in Appendix B), a heuristic path-generation step: the working set $\widetilde{P}_{rs}$ need not contain the minimum-augmented-cost feasible path (Sections 3.3 and 5.3); and (iii) update path flows via closed-form flow balancing.

Augmented Marginal Cost The marginal cost of path $p \in P_{rs}$ under the current shadow prices is

$$\widetilde{C}_p^{rs}(\boldsymbol{\rho}, \beta) \;=\; \sum_{a \in E} \delta_a^{rs,p}\, t_a(x_a, \bar{x}_a^e) \;+\; \sum_{e \in F} \mathbb{1}_{[e \in p]}\, \max\{0,\, \rho_e + \beta(\lambda_e - \alpha \mu_e)\}, \tag{22}$$

where $\mathbb{1}_{[e \in p]} = 1$ iff path p uses charger e.

Path-Flow Balancing Let $p^\star \in \widetilde{P}_{rs}$ denote the basic path of minimum $\widetilde{C}_p^{rs}$. For every non-basic path $p \in \widetilde{P}_{rs} \setminus \{p^\star\}$, the closed-form flow-shift rule used at each inner iteration is

$$\Delta f_p^{rs} \;=\; \min\left\{ f_p^{rs},\; \frac{\widetilde{C}_p^{rs} - \widetilde{C}_{p^\star}^{rs}}{\sum_{a \in p \triangle p^\star} \dfrac{\partial \widetilde{C}}{\partial x_a}} \right\}, \tag{23}$$

where $p \triangle p^\star$ is the symmetric difference of the link sets of p and $p^\star$. The denominator is the sum of own-flow sensitivities along the disjoint links and is positive by strict convexity of (9); this guarantees $\Delta f_p^{rs} > 0$ whenever $\widetilde{C}_p^{rs} > \widetilde{C}_{p^\star}^{rs}$. Note that the gradients in (22) include both direct link effects *and* indirect effects through the shared station inflow λ_e, consistent with the symmetry property of Lemma 1.

5.3 Convergence and Parallelization

The outer multiplier update (19) is the standard augmented-Lagrangian multiplier method for convex programs. Restricted to fixed path sets, (9)–(15) is a convex program with affine constraints, and for this class the multiplier iterates converge to an optimal multiplier vector (with every accumulation point of the primal iterates optimal), provided the inner minimizations are carried out with vanishing (or summable) errors (Hestenes 1969; Powell 1969; Rockafellar 1973; Bertsekas 1982). Strict convexity is not required for this guarantee; it matters only for Theorem 2, which gives uniqueness of the equilibrium link and station flows. Two qualifications delimit the scope of this guarantee. First, the classical result applies to the program whose path sets are given: because Algorithm 1 is a heuristic generator (Section 3.3), the computed point satisfies the KKT conditions of (9)–(15) *restricted to the generated working sets* $\{\widetilde{P}_{rs}\}$ to within the reported tolerances. It is not certified as an equilibrium over the full feasible sets $\{P_{rs}\}$ of Theorem 1. Second, the inner problem is solved inexactly, to the relative-gap tolerance γ_3, so the outer iteration is of the inexact-minimization type. Empirical evidence on the quality of the generated path sets (a comparison against full enumeration of feasible paths on the toy network) is reported in Section 6.2. The inner loop terminates when the standard relative gap between total system cost and feasible-shortest-path cost (Boyles et al. 2020) drops below tolerance γ_3. Because the inner column-generation step decomposes by OD pair at a fixed generalized-cost and price vector, the inner loop parallelizes naturally: OD pairs

are processed on separate workers between cost synchronizations, coordinated by the outer loop (Bertsekas and Tsitsiklis 2015).

6 Numerical Examples

We validate the proposed model and algorithm on four networks of increasing size and report equilibrium properties, computational performance, and supply/demand sensitivity. All experiments were run in Python 3.9 on a desktop with an Intel Xeon^{TM} W-2295 CPU (18 cores, 3.00 GHz) and 128 GB of DDR4 RAM. Convergence tolerances are set to $\gamma_1 = \gamma_2 = \gamma_3 = 10^{-3}$. In all experiments $\alpha = 1$: wherever the capacity constraint (13) is imposed, its bound is the hardware service rate, so the station capacities reported below (e.g., Table 5) are the service rates μ_e themselves. Dwell times are computed from Eq. (3) with $w_e^0 = 1$ (Section 3.4), so that time is measured in units of the base service time and μ_e equals the number of parallel servers at station e; the two toy-network stations of Table 5, for instance, have 30 and 8 servers. Following (Jiang and Xie 2014), the EV range R is scaled with network size so that charging activity is non-trivial in every instance, while the range and the charger deployment together guarantee that every OD pair retains at least one feasible itinerary with at most one charging stop, the scope stated in Section 3.3.

6.1 Test Networks

The four networks are the toy network of Fig. 3 (8 nodes, 9 corridor links, 2 community chargers), the Sioux Falls benchmark, and two real-world networks: Eastern Massachusetts (medium) and Chicago Sketch (large). The two real-world networks are illustrated in Fig. 6; their dimensions are summarized in Table 2, where $|V|$, $|E^{nc}|$, $|E^c|$, $|F|$, and $|W|$ denote the number of nodes, non-connecting links, connecting links, chargers, and OD pairs, respectively. Connecting links are counted in both directions; the inbound subsets that enter the dwell aggregation of Eq. (10) have $|E^{c,\text{in}}| = |E^c|/2$ (Section 3.2). Each network can also be partitioned into spatial subregions, which

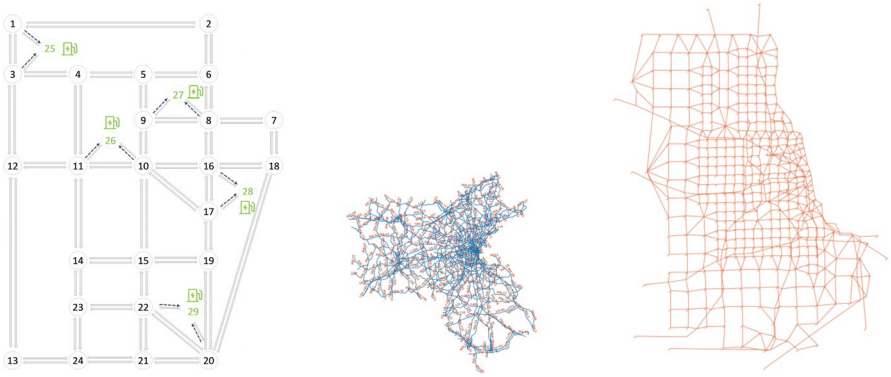


Fig. 6 Real-world test networks used in the numerical experiments: (left) Sioux Falls; (middle) Eastern Massachusetts; (right) Chicago Sketch

Table 2 Sizes of the four test networks

Network	$\|V\|$	$\|E^{nc}\|$	$\|E^{c}\|$	$\|F\|$	$\|W\|$
Toy network	10	9	8	2	2
Sioux Falls	29	76	20	5	528
Eastern Massachusetts	99	258	100	25	1,113
Chicago Sketch	1,221	2,950	1,152	288	93,135

Table 3 Equilibrium path flow distribution for the toy network under the proposed model with the station capacity side constraint (13)

OD	ID	Node sequence	Flow	Travel time	Dwell time	Total cost
(1, 3)	1	1−2−9−2−3	10.40	22.86	2.27	25.13
(1, 3)	2	1−4−9−4−5−3	9.60	22.86	2.27	25.13
(1, 3)	3	1−4−5−10−5−3	0.00	22.87	3.00	25.87
(6, 8)	4	6−4−9−4−5−8	2.00	14.72	2.27	16.99
(6, 8)	5	6−4−5−10−5−8	0.00	14.72	3.00	17.72
(6, 8)	6	6−7−10−7−8	8.00	11.91	3.00	14.91

Table 4 Toy network: converged path flows when the station capacity side constraint (13) is dropped. Used-path costs equalize within each OD pair, but charger 10 is over-capacity (see Table 5)

OD	ID	Node sequence	Flow	Travel time	Dwell time	Total cost
(1, 3)	1	1−2−9−2−3	10.32	22.35	2.24	24.59
(1, 3)	2	1−4−9−4−5−3	9.68	22.34	2.24	24.59
(1, 3)	3	1−4−5−10−5−3	0.00	22.35	3.13	25.49
(6, 8)	4	6−4−9−4−5−8	1.65	13.92	2.24	16.16
(6, 8)	5	6−4−5−10−5−8	0.00	13.93	3.13	17.06
(6, 8)	6	6−7−10−7−8	8.35	13.03	3.13	16.16

makes it suitable for evaluating decentralized implementations based on localized flow assignment.

6.2 Performance on the Toy Network

We first validate equilibrium behavior on the toy network. The path flows at convergence are reported in Table 3. The reported pair of flows and prices satisfies Definition 1 clause by clause. For OD pair (1, 3), both used paths charge at station 9, whose capacity constraint is inactive ($\rho_9 = 0$, Table 5); their augmented costs equal their physical costs and coincide at 25.13, strictly below the unused path's augmented cost ($25.87 + \rho_{10} = 27.94$). For OD pair (6, 8), the two used paths have *different* physical costs (16.99 vs. 14.91), precisely the situation Definition 1 anticipates at a saturated station. Charger 10 is at capacity and carries the price $\rho_{10} = 2.07$: the augmented costs of the two used paths coincide within the rounding of the printed values (16.99 and $14.91 + 2.07 = 16.98$), the unused path's augmented cost is higher ($17.72 + 2.07 = 19.79$), and complementary slackness (8) holds at both stations. Under the pricing reading of Section 3.5, ρ_{10} is the capacity-clearing access charge at the saturated station; under the queueing reading, users of charger 10 perceive a total station delay of $3.00 + 2.07$ time units. For comparison, Table 4 reports the converged flows when the capacity side constraint (13) is dropped; in that case both OD

pairs recover the standard Wardropian equality of used-path costs, but charger 10 is overloaded ($x = 8.35 > \mu_{10} = 8.00$), confirming that the side constraint binds in the original problem.

Completeness of the Working Path Set on the Toy Network A full enumeration of feasible paths from the printed network data (all simple routes with same-access charger insertions and at most one visit per station) yields exactly 4 feasible paths for OD (1, 3) and 4 for OD (6, 8). In each case the paths beyond those listed in Tables 3–4 are two-charge paths, each equal to a listed path plus one pure station round trip (two access-link traversals and one dwell), hence strictly costlier at every flow and price vector, consistent with Proposition 1 and outside the one-stop scope of Section 3.3. After discarding them, the remaining 3 and 3 paths coincide exactly with the working sets of Tables 3–6. On the toy network the heuristic generator therefore loses no undominated feasible path, and the computed equilibrium is an equilibrium over the full feasible set under the station-access conventions (i)–(v) of Section 3.2 (the enumeration is reproducible from the printed network data).

The corresponding station-level statistics are reported in Table 5. Charger 1 (at node 9) operates well below capacity in both runs and has $\rho_9 = 0$, so its constraint is inactive. Charger 2 (at node 10), in contrast, is over capacity when the side constraint is dropped (8.35 vs. a hardware limit of 8.00); under the proposed model the inflow is exactly clipped to 8.00, the constraint is active, and $\rho_{10} = 2.07$. In the language of Section 3.5, ρ_{10} is the time-equivalent capacity-clearing access charge at charger 10 under the pricing reading (the implicit price of rationing at the saturated station), or equivalently the equilibrium delay of the rationing process under the queueing reading.

Comparison with an Interaction-Ignored Baseline We benchmark the proposed algorithm against a path-based gradient- projection algorithm that ignores the demand–service interaction (1) (i.e., treats each connecting-link cost as depending only on its own flow). The converged flows from this baseline are reported in Table 6. For OD (1, 3) the three used paths exhibit distinct total costs at convergence (26.53, 25.70, 26.42), so the baseline does *not* reach equilibrium under the true non-separable costs: shifting flow off path 3 would equalize paths 1–2 and lower the system cost. The mismatch arises precisely because the baseline ignores the cross-link sensitivity through $\partial t_a / \partial x_b$ at charger 10 (Lemma 1), so its descent direction mis-prices each move that shifts flow between connecting links sharing a station.

Table 5 Toy network: equilibrium station inflows and shadow prices. μ_e is the hardware service rate; with $\alpha = 1$ it is also the capacity enforced in (13), and with $w_e^0 = 1$ it is also the number of parallel servers at the station (Section 3.4).

			Without cap. side constraint		With cap. side constraint (proposed)		
Stn.	Node	μ_e	Flow	Dwell	Flow	Dwell	ρ_e
1	9	30.00	21.65	2.24	22.00	2.27	0
2	10	8.00	8.35	3.13	8.00	3.00	2.07

Table 6 Toy network: converged path flows under the interaction-ignored gradient-projection baseline. Used-path costs do *not* equalize for either OD pair, so the baseline does not satisfy the generalized UE conditions of (6)–(7)

OD	ID	Node sequence	Flow	Travel time	Dwell time	Total cost
(1, 3)	1	1−2−9−2−3	10.61	24.25	2.28	26.53
(1, 3)	2	1−4−9−4−5−3	8.84	23.43	2.28	25.70
(1, 3)	3	1−4−5−10−5−3	0.55	23.44	2.98	26.42
(6, 8)	4	6−4−9−4−5−8	2.61	16.00	2.28	18.28
(6, 8)	5	6−4−5−10−5−8	0.00	16.01	2.98	18.99
(6, 8)	6	6−7−10−7−8	7.39	10.32	2.98	13.29

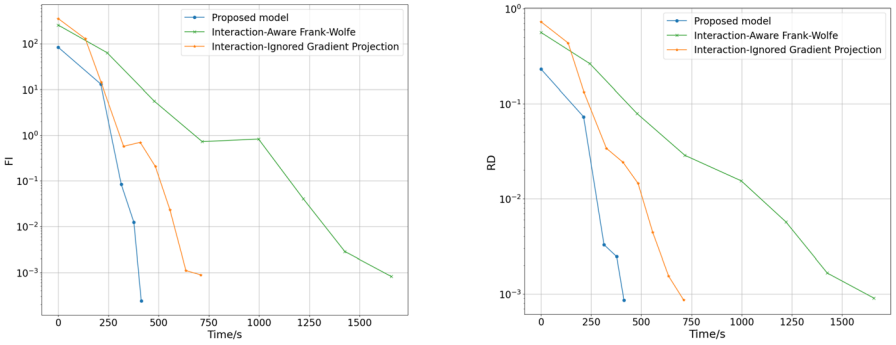


Fig. 7 Convergence of the proposed ALM–CG algorithm and the two baselines on the Chicago Sketch network. Left: flow infeasibility FI vs. wall-clock time. Right: relative duality difference RD vs. wall-clock time

6.3 Computational Performance

We compare three solvers on each network: (a) the proposed augmented-Lagrangian column-generation (ALM–CG) algorithm; (b) the interaction-ignored gradient-projection baseline of Section 6.2; and (c) an interaction-aware Frank–Wolfe algorithm, a link-based equilibrium method that retains the demand–service coupling. For a fair comparison, both baselines are wrapped in the same outer augmented-Lagrangian loop so that the station capacity constraint is enforced in all three solvers; only the inner equilibrium step differs.

Figure 7 shows the convergence of all three solvers on the largest test network (Chicago Sketch). The proposed ALM–CG algorithm drives both the flow infeasibility (FI) and the relative duality difference (RD) below the tolerance considerably faster than either baseline; the bulk of the gain occurs within the first 500 seconds and 5 outer iterations. The interaction-ignored gradient projection comes second by virtue of its path-based structure; the link-based interaction-aware Frank–Wolfe algorithm is the slowest, exhibiting the method's characteristic slow tail convergence.

Wall-clock times across all four networks are summarized in Table 7. The proposed algorithm is roughly 30–42% faster than the interaction-ignored gradient projection across the four networks and roughly 75% faster than the interaction-aware Frank–Wolfe algorithm on Chicago Sketch (about a quarter of the Frank–Wolfe wall-clock

Table 7 Wall-clock time (seconds) of the proposed algorithm and the two benchmarks across the four test networks

Network	Proposed ALM–CG	Interaction-ignored gradient projection	Interaction-aware Frank–Wolfe
Toy network	0.67	0.96	2.43
Sioux Falls	5.81	9.42	19.86
Eastern Massachusetts	57.95	99.08	142.13
Chicago Sketch	413.40	710.19	1657.63

time). The absolute time saved grows rapidly with network size, from about 2 s on the toy network to over 1200 s on Chicago Sketch: the ALM–CG cost is dominated by the parallel inner column-generation step, whereas Frank–Wolfe re-evaluates the interaction-aware link costs network-wide and computes a full all-or-nothing assignment at every iteration.

6.4 Sensitivity to Charging Supply and Demand

To examine how the equilibrium responds to changes in the resource and demand layers, we vary (i) the station capacity μ_e by a common scale factor in $\{0.2, 0.4, 0.6, 0.8\}$ (with $w_e^0 = 1$ fixed, so that the factor scales the number of servers $c_e = \mu_e$ of Section 3.4, treated here as a continuous capacity parameter) and (ii) the OD demand q^{rs} by the same set of factors, and report total system travel cost and total system dwell time on the Eastern Massachusetts network.

Figure 8(a,b) shows the response to changing supply. Both total travel cost and total dwell time fall monotonically as capacity increases, with the dwell-time decrease flattening at higher capacity levels, consistent with the quadratic shape of the polynomial dwell function (3). The travel-time component (the gap between the two curves) is essentially flat, indicating that station-capacity changes propagate primarily through the dwell-time term, not through link travel times.

Figure 8(c,d) shows the response to changing demand. Both total travel cost and dwell time increase with demand, and dwell time rises faster than linearly, mirroring the quadratic flow term in (3). Across both experiments the equilibrium responses are sign-consistent with intuition and with the convexity properties of the underlying program.

7 Conclusions

We formulated community charging as a capacity-constrained spatial equilibrium problem in which OD-level routing decisions are linked through shared station-level capacity constraints and through non-separable, flow–service-coupled link costs. The model captures two structural features that distinguish community charging from corridor charging: (F1) many-to-one flow–service coupling, where flows from different OD pairs and routes converge on the same charger via overlapping local arterials; and (F2) shared station capacity that simultaneously constrains every OD pair using a given charger. We proved that the program is exactly a side-constrained Beckmann

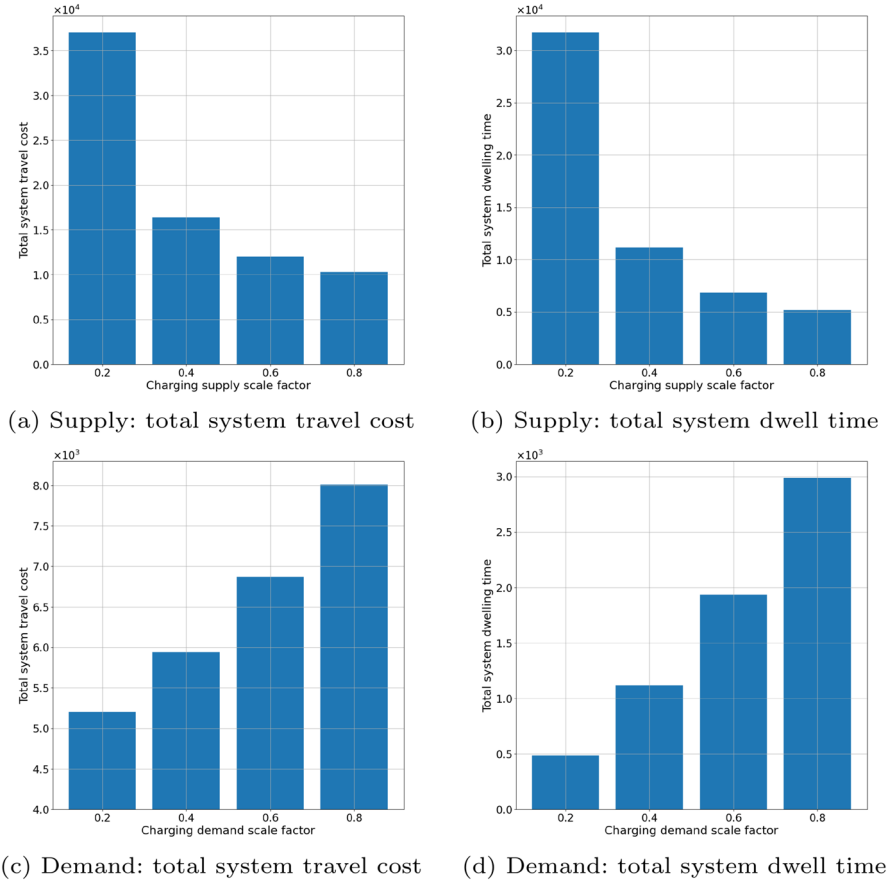


Fig. 8 Sensitivity of the equilibrium to charging supply (top row) and charging demand (bottom row), on the Eastern Massachusetts network. Panels (a,b): total system travel cost and total system dwell time vs. supply scale factor. Panels (c,d): total system travel cost and total system dwell time vs. demand scale factor.

program on a station-expanded network restricted to range- and access-feasible paths (Proposition 2), with the cross-link symmetry (Lemma 1) as the physical-network certificate of the potential. We showed that its KKT solution coincides with a capacity-constrained generalized user equilibrium (path flows together with capacity-clearing station prices) whose link and station flows are unique under strict convexity (Theorems 1–2).

To solve the program we developed a primal–dual decomposition: an outer augmented-Lagrangian loop adjusts station-level shadow prices on capacity, and an inner column-generation loop solves parallelizable path-flow subproblems for each OD pair under the current prices. The shadow prices act as economic coordination signals between network-level capacity scarcity and OD-level routing.

What distinguishes community charging within side-constrained assignment is not the cost structure but three ingredients: the admissible path family (range feasibility

with recharge, and the station-access discipline of Section 3.2); the queueing origin of both the station service cost w_e and the stability capacity $\alpha\mu_e$, which ties the congestion term and the constraint to the same physical model; and the station-indexed prices ρ_e, whose equilibrium reading (the capacity-clearing price of access to a saturated community facility, realized as a posted access charge or as rationing delay) carries the spatial-economic content of the model.

Numerical experiments on four networks of increasing size (toy, Sioux Falls, Eastern Massachusetts, Chicago Sketch) showed that the proposed algorithm reaches equilibrium (to the reported tolerances) under active capacity constraints where a path-based interaction-ignored baseline does not, and runs 30–42% faster than that baseline across the four networks and roughly 75% faster than an interaction-aware Frank–Wolfe algorithm on the largest network, with the absolute time saved growing rapidly as network size grows. Sensitivity analyses confirmed that total system travel cost and aggregate dwell time decrease with charging supply and increase with charging demand, consistent with the convexity of the underlying program.

The proposed framework admits several methodological openings. Because the inner column-generation step decomposes by OD pair, the algorithm extends naturally to a fully distributed implementation in which subregions exchange only boundary flows and shadow prices, along the lines of Bertsekas and Tsitsiklis (2015). A dynamic extension is the most substantial opening, and it would not be a reparameterization of the present model. Over time, vehicles occupy a station for a nonzero service duration, so station inflow, occupancy, and outflow generally differ. The link-based aggregation that is consistent under steady state (Section 3.1) would have to be replaced by explicit station-state conservation and queue evolution, together with a distinction between pre-charging and post-charging link flows. The static equilibrium developed here is the fixed point that such a dynamic model should recover at stationarity. A second extension is to itineraries with two or more charging stops, as on long trips across several states: the generator of Algorithm 1 would then apply its insertion step repeatedly, re-splitting the itinerary at each new stop and re-checking every subpath, while the equilibrium conditions and the algorithm of Section 5 carry over unchanged, since they require only a finite admissible path family. The deterministic OD demand can be replaced by a stochastic process to capture day-to-day arrival variability, and chargers can be coupled to renewable supply with time-varying service rates $\mu_e(t)$. Equity and reliability metrics can also be embedded directly in the spatial-equilibrium objective to support NEVI/CFI-style investment and policy analyses on community-charging networks.

Table 8 Notation used throughout the paper, organized by sets and indices, parameters, decision and derived variables, dual variables and slacks, and convergence measures

Symbol	Meaning
Sets and indices	
$G = (V, E, F)$	Network with nodes V, links E, chargers F
E^c, E^{nc}	Connecting (station-access) / non-connecting link subsets, $E = E^c \cup E^{nc}$
$E^{c,\text{in}}$	Inbound access links (terminating at a charger); $\lvert E^{c,\text{in}}\rvert = \lvert E^c\rvert/2$
W	Set of OD pairs (r, s)
P_{rs}	Set of feasible paths for OD pair (r, s), each with at most one charging stop (Section 3.3)
$\widetilde{P}_{rs}$	Working (active) feasible-path set for (r, s) used by column generation
G'	Station-expanded network (Section 4.2)
e^-, e^+; a_e	Entry/exit ports of charger e; service arc (e^-, e^+)
y_e; Π'_{rs}	Service-arc flow $(= \lambda_e)$; admissible paths $T(P_{rs})$ on G'
a, e, p, (r, s)	Indices for link, charger, path, and OD pair
Parameters	
R	EV battery range
t_a^0, C_a	Free-flow travel time and capacity of link a
α_{BPR}, β_{BPR}	BPR calibration parameters (0.15 and 4)
μ_e	Service-rate (hardware) capacity of charger e, in vehicles per unit time
w_e^0	Base (uncongested) service time of charger e, in time units $(= 1$ in all experiments)
c_e	Number of parallel servers (charging points) at charger e, $c_e = w_e^0 \mu_e$ $(= \mu_e$ in all experiments)
$\alpha \in (0, 1]$	Capacity safety factor ($\alpha = 1$ in all experiments)
q^{rs}	Travel demand for OD pair (r, s)
δ_{ae}	$= 1$ if link a terminates at charger e, else 0
$\delta_a^{rs,p}$	$= 1$ if link a lies on path $p \in P_{rs}$, else 0
$\beta > 0$, $\xi > 1$, $\iota \in (0, 1)$	Augmented-Lagrangian penalty and update parameters
$\gamma_1, \gamma_2, \gamma_3$	Convergence tolerances for FI, RD, and the relative gap
Decision and derived variables	
f_p^{rs}	Flow on path $p \in P_{rs}$
x_a	Flow on link a derived from path flows by (11)
λ_e	Aggregate inflow to charger e defined by (10)
$\bar{x}_a^e$	Inflow to charger e from connecting links other than a
$t_a^{\text{road}}(x_a)$	BPR road travel time on link a
$w_e(\lambda_e)$	Dwell time at charger e (polynomial form (3))
$t_a(x_a, \bar{x}_a^e)$	Generalized link cost (1)
C_p^{rs}, $\widetilde{C}_p^{rs}$	Generalized and shadow-price-augmented path costs
$\widehat{C}_p^{rs}$	Augmented path cost, Eq. (5) (Definition 1)
$\mathbb{1}_{[e \in p]}$	Indicator equal to 1 if path p uses charger e, 0 otherwise
$Z(\boldsymbol{f})$	Generalized Beckmann potential (9)
Dual variables and slacks	
ρ_e	Station-level shadow price on capacity at charger e
u^{rs}	Multiplier on the demand-conservation constraint of OD (r, s)

Table 8 (continued)

Symbol	Meaning
$s_e \geq 0$	Slack on the capacity inequality (16)
$\mathcal{L}(\boldsymbol{f}, \boldsymbol{\rho}, \boldsymbol{u})$	Lagrangian of (9)–(15), see (A1)
$L_\beta(\cdot)$	Augmented Lagrangian (18)
Convergence measures	
FI	Flow infeasibility, $\sum_e \max\{0, \lambda_e - \alpha\mu_e\}$
RD	Relative duality difference between L_β and Z
RG	Relative gap between total system cost and feasible shortest-path cost

Table 9 Single-server case ($c_e = 1$): exact M/M/1 dwell time versus its second-order truncation (3), in units of $1/\mu_e$. The truncation retains the share $1 - \theta^3$ of the exact delay, independently of μ_e

$\theta = \lambda_e/\mu_e$	Exact $\frac{1}{1-\theta}$	Truncated $1+\theta+\theta^2$	Retained share $1 - \theta^3$	Underestimation θ^3 (%)
0.5	2.00	1.75	0.875	12.5
0.7	3.33	2.19	0.657	34.3
0.8	5.00	2.44	0.488	51.2
0.9	10.00	2.71	0.271	72.9
0.95	20.00	2.85	0.143	85.7

Appendix A: Notation

Appendix B: Proofs and Derivations

B.1 Polynomial Approximation of the Dwell Time

For a single-server station ($c_e = 1$, so that $w_e^0 = 1/\mu_e$; Section 3.4), the $M/M/1$ dwell time at charger e with arrival rate λ_e and service rate μ_e is $w_e(\lambda_e) = (\mu_e - \lambda_e)^{-1}$. Its derivatives evaluated at $\lambda_e = 0$ are

$$w_e(0) = \frac{1}{\mu_e}, \quad w_e'(0) = \frac{1}{\mu_e^2}, \quad w_e''(0) = \frac{2}{\mu_e^3}.$$

The second-order Taylor expansion at $\lambda_e = 0$ is therefore

$$w_e(\lambda_e) \approx \frac{1}{\mu_e} + \frac{\lambda_e}{\mu_e^2} + \frac{\lambda_e^2}{\mu_e^3},$$

which is (3) with $w_e^0 = 1/\mu_e$. The polynomial is convex in λ_e for $\mu_e > 0$ and exact up to $O(\lambda_e^3)$. In this single-server case the truncation error admits a closed form: since $(1 + \theta + \theta^2)(1 - \theta) = 1 - \theta^3$ with $\theta = \lambda_e/\mu_e$, the truncated dwell time retains exactly the share $1 - \theta^3$ of the exact M/M/1 delay and underestimates it by the fraction θ^3 , uniformly in μ_e. Table 9 tabulates the gap: it is modest at low utilization (12.5% at $\theta = 0.5$) but substantial near capacity (72.9% at $\theta = 0.9$), and the exact delay diverges as $\theta \to 1$. The truncation is therefore *not* intended as an accurate delay model near saturation. It deliberately replaces the singularity by a stable convex polynomial, and congestion beyond the truncation is handled by the capacity constraint (13) and its price ρ_e. At a binding station, additional cost is no longer described by the dwell function at all: it emerges endogenously as the price ρ_e that rations arrivals to capacity (the pricing reading of Section 3.5; under the queueing reading, that price is realized as rationing delay). The omitted M/M/1 tail and ρ_e play the same role but are not numerically equal: ρ_e is set by the equilibrium conditions, not by the M/M/1 formula, whose value at a binding station with $\alpha = 1$ would be unbounded while

ρ_e remains finite. In this respect the polynomial functions as a station-side volume–delay function in the same spirit as the BPR function on road links (finite at capacity by design, with scarcity priced by the constraint) rather than as an estimator of the M/M/1 curve near saturation. None of the theoretical results depends on the truncation order: Lemma 1 and Theorems 1–2 require only a smooth, nondecreasing dwell function of the aggregate inflow, so a higher-order truncation (or a different convex delay function) can be substituted, with no change to the theory, where an application demands tighter fidelity at intermediate utilization. At the enforced utilization bound $\theta = \alpha$, the omitted share is α^3, which quantifies the trade-off between approximation fidelity and usable capacity set by the choice of the safety factor.

For $c_e > 1$ (under $w_e^0 = 1$, every station with $\mu_e > 1$, such as the stations of Table 5), (3) is used as a volume–delay function in its own right (Section 3.4); it is not a truncation of the exact multi-server delay, and the closed-form error above and Table 9 do not apply to it. The design argument is the same for every c_e: a finite convex delay curve, with scarcity at capacity priced by the constraint.

B.2 Proof of Proposition 1

Consider an EV with two feasible alternatives between origin and destination: charging once at station $e_1 or e_2$, versus charging twice at $bothe_1$ and e_2. Let ΔE be the total energy required and let charging speeds (kW) be σ_1 and σ_2 at the two stations, with waiting times w_1, w_2. If energies η_1, η_2 are charged with $\eta_1 + \eta_2 = \Delta E$, the two-stop charging time is $T_2 = w_1 + \eta_1/\sigma_1 + w_2 + \eta_2/\sigma_2$. The single-stop times at e_i are $T_i = w_i + \Delta E/\sigma_i$. A direct computation gives

$$T_2 - \min\{T_1, T_2\} \;=\; \max\left\{\eta_2\left(\frac{1}{\sigma_2} - \frac{1}{\sigma_1}\right) + w_2,\; \eta_1\left(\frac{1}{\sigma_1} - \frac{1}{\sigma_2}\right) + w_1\right\} \;\geq\; 0,$$

since at least one of the two terms is non-negative (whichever station has the higher speed dominates). Hence charging once is weakly preferred whenever it is feasible.□

B.3Proof of Proposition 2 (station-expanded equivalence)

Fix an OD pair (r, s). By conventions (i)–(v) of Section 3.2, a feasible path $p \in P_{rs}$ traverses each directed link at most once and charges at each station at most once, so its image $T(p)$, each visit $v \to e \to v$ replaced by $v \to e^- \to e^+ \to v$, is a well-defined path of G'. The map T is a bijection between P_{rs} and Π'_{rs}, with inverse given by contracting each $v \to e^- \to e^+ \to v$ back to $v \to e \to v$. Service arcs have zero length and carry the recharge, so p and $T(p)$ have identical subpath lengths and range feasibility is preserved in both directions. Assign $T(p)$ the flow f_p^{rs}. Every image road arc then carries exactly the flow x_a of its preimage link (Eq. (11)), and the service-arc flow satisfies

$$y_e \;=\; \sum_{(r,s)\in W} \sum_{p\in P_{rs}} \mathbb{1}_{[e\in p]}\, f_p^{rs} \;=\; \sum_{a\in E^{c,\text{in}}} \delta_{ae}\, x_a \;=\; \lambda_e,$$

the middle equality holding because, by conventions (ii) and (iv)–(v), a path charges at e if and only if it uses exactly one inbound access link of e, exactly once. The two objectives therefore agree term by term: the road sums range over the same links with the same costs and flows, and the station term $\sum_e \int_0^{\lambda_e} w_e$ of (9) is the separable arc integral $\sum_e \int_0^{y_e} w_e$ on G'. The constraints correspond one to one under T: demand conservation (14) and non-negativity (15) transfer verbatim, and the station capacity (13) is the arc capacity $y_e \le \alpha\mu_e$ of a_e. Two programs with the same decision variables (after the identification T), the same objective, and the same constraints have the same Lagrangian and hence the same KKT system; the multiplier of (13) and the capacity dual of a_e are the same object.□

B.4 Proof of Lemma 1 (cross-link symmetry)

For two inbound access links $a, b \in E^{c,\text{in}}$ both terminating at charger e, the polynomial dwell-time function (3) gives

$$\frac{\partial t_a}{\partial x_b} \;=\; \frac{\partial w_e(\lambda_e)}{\partial \lambda_e} \cdot \frac{\partial \lambda_e}{\partial x_b} \;=\; w_e^0 \left(\frac{1}{\mu_e} + \frac{2\lambda_e}{\mu_e^2} \right) \cdot 1,$$

and by the same calculation $\partial t_b / \partial x_a = w_e^0 \, (1/\mu_e + 2\lambda_e/\mu_e^2) \cdot 1$. Therefore $\partial t_a / \partial x_b = \partial t_b / \partial x_a$.□

B.5 Proof of Theorem 1: KKT ⇔ generalized UE

The Lagrangian of (9)–(15) with multipliers $\rho_e \ge 0$ on the capacity constraint (13) and u^{rs} on the demand constraint (14) is

$$\mathcal{L}(\boldsymbol{f}, \boldsymbol{\rho}, \boldsymbol{u}) \;=\; Z(\boldsymbol{f}) \;+\; \sum_{e \in F} \rho_e (\lambda_e - \alpha\mu_e) \;-\; \sum_{(r,s) \in W} u^{rs} \left(\sum_p f_p^{rs} - q^{rs} \right). \tag{A1}$$

Differentiating with respect to f_p^{rs} and using the chain rule together with (11) and (10) yields

$$\frac{\partial \mathcal{L}}{\partial f_p^{rs}} \;=\; C_p^{rs} \;+\; \sum_{e \in F} \mathbb{1}_{[e \in p]} \, \rho_e \;-\; u^{rs}. \tag{A2}$$

The KKT conditions of the convex program are

$$f_p^{rs} \left(C_p^{rs} + \sum_e \mathbb{1}_{[e \in p]} \rho_e - u^{rs} \right) = 0, \quad \forall (r,s),\ p, \tag{A3}$$

$$C_p^{rs} + \sum_e \mathbb{1}_{[e \in p]} \rho_e - u^{rs} \ge 0, \quad \forall (r,s),\ p, \tag{A4}$$

$$\rho_e(\lambda_e - \alpha\mu_e) = 0, \quad \rho_e \geq 0, \ \ \lambda_e \leq \alpha\mu_e, \quad \forall e. \tag{A5}$$

The cost appearing in (A3)–(A4) is exactly the augmented path cost $\widehat{C}_p^{rs}(\boldsymbol{\rho})$ of Eq. (5). Hence (A3)–(A4) are conditions (6)–(7) of Definition 1 with u^{rs} the minimum augmented cost, and (A5) is primal feasibility of (13) together with the complementary-slackness condition (8). The capacity charge ρ_e is positive only when the corresponding station is saturated ($\rho_e > 0 \Rightarrow \lambda_e = \alpha\mu_e$), recovering the pricing reading of Section 3.5. The program (9)–(15) is convex and all of its constraints (10)–(15) are affine in $\boldsymbol{f}$, so no constraint qualification beyond feasibility is required: whenever the feasible set is nonempty, the KKT conditions (A3)–(A5) are both necessary and sufficient for optimality (Bertsekas 2015). Combined with the equivalence just established, this gives the if-and-only-if statement of Theorem 1.□

B.6 Proof of Theorem 2 (uniqueness)

Convexity of Z implies uniqueness of the link-flow vector $\boldsymbol{x}^*$ on the feasible region. We show convexity by computing the Hessian. For links that carry only road time (non-connecting links and outbound access links), the contribution to the Hessian is the diagonal block $H_{nc} = \mathrm{diag}\big((t_a^{\mathrm{road}})'(x_a)\big)$, which is positive semidefinite because the BPR function is non-decreasing, with $(t_a^{\mathrm{road}})'(x_a) \geq 0$ and strictly positive for $x_a > 0$. For inbound access links $a, b \in E^{c,\mathrm{in}}$ sharing charger e, the 2×2 block of $\partial^2 Z / \partial x_a \partial x_b$ is

$$H_e \;=\; \begin{pmatrix} (t_a^{\mathrm{road}})'(x_a) + w_e'(\lambda_e) & w_e'(\lambda_e) \\ w_e'(\lambda_e) & (t_b^{\mathrm{road}})'(x_b) + w_e'(\lambda_e) \end{pmatrix}.$$

The diagonal entries are bounded below by $w_e'(\lambda_e) = w_e^0\,(1/\mu_e + 2\lambda_e/\mu_e^2) > 0$. The determinant of H_e equals

$$(t_a^{\mathrm{road}})'(x_a)\,(t_b^{\mathrm{road}})'(x_b) + w_e'(\lambda_e)\Big[(t_a^{\mathrm{road}})'(x_a) + (t_b^{\mathrm{road}})'(x_b)\Big] \;\geq\; 0,$$

and is strictly positive whenever $(t_a^{\mathrm{road}})'(x_a) + (t_b^{\mathrm{road}})'(x_b) > 0$, which holds at any link with positive flow. Hence H_e is positive definite on the positive orthant and positive semidefinite at the boundary. Every 2×2 diagonal block of the full Hessian is positive definite and the cross-block second partials vanish, so $H = \mathrm{diag}(H_{nc}, H_e \text{ blocks})$ is positive definite. Strict convexity of Z over the convex feasible set then yields uniqueness of the optimal link-flow vector $\boldsymbol{x}^*$. Path flows are not necessarily unique, but any equilibrium path-flow decomposition reproduces $\boldsymbol{x}^*$ via (11).□

k-shortest feasible-path algorithm

Require: Network $G = (V, E, F)$, EV range R, OD pair (r, s), candidate count k.
Set $\widetilde{P}_{rs} \leftarrow \emptyset$. Compute k-shortest paths from r to s on the base road network (G with charger nodes and access links removed) using Yen's algorithm.
for each candidate path p **do**
  if the length of p is at most R **then**
    Add p to $\widetilde{P}_{rs}$: it is feasible without charging.
  else
    for each node v on p and each charger $e \in F$ with $(v, e) \in E^{c,\text{in}}$ **do**
      Form $p_{v,e}$ by inserting the same-access round trip $v \to e \to v$ into p at v (one charging stop at e; Section 3.2).
      if the two subpaths of $p_{v,e}$, from r to e and from e to s, both have length at most R **then**
        Add $p_{v,e}$ to $\widetilde{P}_{rs}$.
      end if
    end for
    If no $p_{v,e}$ was added, p contributes no itinerary: a second stop lies outside the scope of Section 3.3.
  end if
end for
return $\widetilde{P}_{rs}$.

Algorithm 1 *k*-shortest feasible-path generation for one OD pair (r, s), itineraries with at most one charging stop (Section 3.3)

The generated itineraries satisfy the station-access conventions of Section 3.2 by construction: the base paths are simple paths of the road-only network and therefore visit no charger, and each itinerary contains at most one same-access round trip, on two distinct directed links, so conventions (iv) and (v) hold without a separate filter; a stop is inserted only into a road path that is infeasible without it, so no itinerary carries a redundant stop in the sense of Proposition 1. The procedure makes one insertion trial per pair of an access node on p and a charger reachable from it, keeps every trial that restores range feasibility, and discards a candidate for which no trial does; since the scope of Section 3.3 excludes a second stop, no further repair is attempted. The three itineraries of OD pair (1, 3) in Table 3 arise in this way from the two road paths $1-2-3$ and $1-4-5-3$ of Fig. 3: the first admits the stop at station 9 from node 2, the second the stops at station 9 from node 4 and at station 10 from node 5.

Acknowledgements No generative AI tools were used to create scientific content, formulate methods, derive equations, analyze data, or develop conceptual or technical ideas in this manuscript. All modeling, derivations, interpretations, and conclusions were produced entirely by the authors. Generative AI tools (e.g., ChatGPT) were used only for language proofreading and minor editorial improvements, and the authors take full responsibility for the final content.

Author Contributions Yang Song: Formal analysis, Validation, Visualization, Writing — original draft. Xianbiao Hu (corresponding author): Conceptualization, Methodology, Supervision, Writing — original draft. Peiheng Li: Validation, Editing — original draft. Xuesong (Simon) Zhou: Conceptualization, Methodology, Editing — original draft. All authors reviewed and approved the final version of the manuscript.

Funding The authors did not receive support from any organization for the submitted work. No funding was received to assist with the preparation of this manuscript, and no funding was received for conducting this study.

Data Availability No datasets were generated or analysed during the current study.

Code Availability Implementation code and analysis scripts will be made available upon reasonable request to the corresponding author and, conditional on acceptance, deposited in a public repository with the manuscript's DOI.

Declarations

Ethical Approval Not applicable. This study did not involve human participants, human data, or animals.

Conflicts of Interest The authors have no relevant financial or non-financial interests to disclose. The authors declare that they have no known competing financial interests or personal relationships that could have appeared to influence the work reported in this paper.

Open Access This article is licensed under a Creative Commons Attribution 4.0 International License, which permits use, sharing, adaptation, distribution and reproduction in any medium or format, as long as you give appropriate credit to the original author(s) and the source, provide a link to the Creative Commons licence, and indicate if changes were made. The images or other third party material in this article are included in the article's Creative Commons licence, unless indicated otherwise in a credit line to the material. If material is not included in the article's Creative Commons licence and your intended use is not permitted by statutory regulation or exceeds the permitted use, you will need to obtain permission directly from the copyright holder. To view a copy of this licence, visit http://creativecommons.org/licenses/by/4.0/.

References

Bell MG (1995) Stochastic user equilibrium assignment in networks with queues. Transport Res Part B Methodol 29(2):125–137

Bertsekas DP (1982) Constrained optimization and lagrange multiplier methods. Academic Press, New York

Bertsekas DP (2015) convex optimization algorithms. Athena Scientif

Bertsekas DP, Tsitsiklis JN (2015) Parallel and distributed computation: Numerical methods. Athena Scientif

Bifulco GN (1993) A stochastic user equilibrium assignment model for the evaluation of parking policies. Eur J Oper Res 71(2):269–287

Boyles SD, Tang S, Unnikrishnan A (2015) Parking search equilibrium on a network. Transport Res Part B Methodol 81:390–409

Boyles SD, Lownes NE, Unnikrishnan A (2020) Transportation network analysis, Volume I. Version 0. p 85

Bureau of Public Roads (1964) Traffic assignment manual for application with a large, high speed computer. Tech. rep., U.S. Department of Commerce, Bureau of Public Roads, Office of Planning, Urban Planning Division, Washington, D.C

Capar I, Kuby M, Leon VJ et al (2013) An arc cover-path-cover formulation and strategic analysis of alternative-fuel station locations. Eur J Oper Res 227(1):142–151

Cardinali S, Epstein A, Thurstin L et al (2023) Webinar: Community charging models. https://driveelectric.gov/webinars/community-charging

Cavadas J, de Almeida Correia GH, Gouveia J (2015) A MIP model for locating slow-charging stations for electric vehicles in urban areas accounting for driver tours. Transport Res Part E Logist Transport Rev 75:188–201

Chen Z, Deng Y, Xie C et al (2023) Network equilibrium of battery electric vehicles considering drivers' resting behavior. Transport Res Part C Emerg Technol 155:104305

Cominetti R, Correa J (2001) Common-lines and passenger assignment in congested transit networks. Transp Sci 35(3):250–267

Dafermos S (1980) Traffic equilibrium and variational inequalities. Transp Sci 14(1):42–54

Dafermos SC (1971) An extended traffic assignment model with applications to two-way traffic. Transp Sci 5(4):366–389

Daganzo CF (1977) On the traffic assignment problem with flow dependent costs–I. Transp Res 11(6):433–437
Daganzo CF (1977) On the traffic assignment problem with flow dependent costs–II. Transp Res 11(6):439–441
De Cea J, Fernández E (1993) Transit assignment for congested public transport systems: An equilibrium model. Transp Sci 27(2):133–147
Feng L, Xie J, Nie YM et al (2020) Efficient algorithm for the traffic assignment problem with side constraints. Transp Res Rec 2674(4):129–139
Ferrari P (1997) Capacity constraints in urban transport networks. Transport Res Part B Methodol 31(4):291–301
He F, Wu D, Yin Y et al (2013) Optimal deployment of public charging stations for plug-in hybrid electric vehicles. Transport Res Part B Methodol 47:87–101
He F, Yin Y, Lawphongpanich S (2014) Network equilibrium models with battery electric vehicles. Transport Res Part B Methodol 67:306–319
He SY, Kuo YH, Wu D (2016) Incorporating institutional and spatial factors in the selection of the optimal locations of public electric vehicle charging facilities: A case study of Beijing, China. Transport Res Part C Emerg Technol 67:131–148
Hestenes MR (1969) Multiplier and gradient methods. J Optim Theory Appl 4(5):303–320
Hodgson MJ (1990) A flow-capturing location-allocation model. Geogr Anal 22(3):270–279
Huang Y, Kockelman KM (2020) Electric vehicle charging station locations: Elastic demand, station congestion, and network equilibrium. Transp Res Part D: Transp Environ 78:102179
Jayakrishnan R, Tsai WK, Prashker JN et al (1994) Faster path-based algorithm for traffic assignment. Transp Res Rec 1443:75–83
Jiang N, Xie C (2014) Computing and analyzing mixed equilibrium network flows with gasoline and electric vehicles. Comput-Aided Civil Infrastruct Eng 29(8):626–641
Jiang N, Xie C, Waller ST (2012) Path-constrained traffic assignment: model and algorithm. Transp Res Rec 2283(1):25–33
Jiang N, Xie C, Duthie JC et al (2014) A network equilibrium analysis on destination, route and parking choices with mixed gasoline and electric vehicular flows. EURO J Transport Logist 3(1):55–92
Lam WH, Li ZC, Huang HJ et al (2006) Modeling time-dependent travel choice problems in road networks with multiple user classes and multiple parking facilities. Transport Res Part B Methodol 40(5):368–395
Larsson T, Patriksson M (1995) An augmented lagrangean dual algorithm for link capacity side constrained traffic assignment problems. Transport Res Part B Methodol 29(6):433–455
Larsson T, Patriksson M (1999) Side constrained traffic equilibrium models– analysis, computation and applications. Transport Res Part B Methodol 33(4):233–264
Larsson T, Patriksson M, Rydergren C (2004) A column generation procedure for the side constrained traffic equilibrium problem. Transport Res Part B Methodol 38(1):17–38
Little JDC (1961) A proof for the queuing formula: $L = \lambda W$. Oper Res 9(3):383–387
Liu Z, Song Z (2018) Network user equilibrium of battery electric vehicles considering flow-dependent electricity consumption. Transport Res Part C Emerg Technol 95:516–544
Marcotte P, Nguyen S, Schoeb A (2004) A strategic flow model of traffic assignment in static capacitated networks. Oper Res 52(2):191–212
Meng Q, Lam WHK, Yang L (2008) General stochastic user equilibrium traffic assignment problem with link capacity constraints. J Adv Transp 42(4):429–465
Needell ZA, McNerney J, Chang MT et al (2016) Potential for widespread electrification of personal vehicle travel in the United States. Nat Energy 1(9):16112
Nie Y, Zhang H, Lee DH (2004) Models and algorithms for the traffic assignment problem with link capacity constraints. Transport Res Part B Methodol 38(4):285–312
Powell MJD (1969) A method for nonlinear constraints in minimization problems. In: Fletcher R (ed) Optimization. Academic Press, London, pp 283–298
Rockafellar RT (1973) The multiplier method of Hestenes and Powell applied to convex programming. J Optim Theory Appl 12(6):555–562
Rosenthal RW (1973) A class of games possessing pure-strategy Nash equilibria. Internat J Game Theory 2(1):65–67
Shahpar AH, Aashtiani HZ, Babazadeh A (2008) Dynamic penalty function method for the side constrained traffic assignment problem. Appl Math Comput 206(1):332–345

Sheffi Y (1985) Urban Transportation Networks: Equilibrium Analysis with Mathematical Programming Methods. Prentice-Hall, Englewood Cliffs, NJ
Smith M (1979) The existence, uniqueness and stability of traffic equilibria. Transport Res Part B Methodol 13(4):295–304
Stephens-Romero SD, Brown TM, Kang JE et al (2010) Systematic planning to optimize investments in hydrogen infrastructure deployment. Int J Hydrogen Energy 35(10):4652–4667
U.S. Department of Energy (2024) FOTW #1375: Median EV range in model year 2024 reached a record high of 283 miles per charge. https://www.energy.gov/cmei/vehicles/articles/fotw-1375-december-30-2024-median-ev-range-model-year-2024-reached-record, vehicle Technologies Office, Transportation Fact of the Week, 30 December 2024
USDOT (2023a) Charging and fueling infrastructure grant program. https://www.fhwa.dot.gov/bipartisan-infrastructure-law/cfi.cfm, retrieved 10 June 2023
USDOT (2023b) National electric vehicle infrastructure formula program. https://www.fhwa.dot.gov/bipartisan-infrastructure-law/nevi_formula_program.cfm
Velkovski B, Gjorgievski VZ, Markovski B et al (2024) A framework for shared EV charging in residential renewable energy communities. Renew Energ 231:120897
Wang TG, Xie C, Xie J et al (2016) Path-constrained traffic assignment: A trip chain analysis under range anxiety. Transport Res Part C Emerg Technol 68:447–461
Wang YW, Lin CC (2009) Locating road-vehicle refueling stations. Transport Res Part E Logist Transport Rev 45(5):821–829
Xie C, Jiang N (2016) Relay requirement and traffic assignment of electric vehicles. Comput-Aided Civil Infrastruct Eng 31(8):580–598
Xu M, Meng Q, Liu K (2017) Network user equilibrium problems for the mixed battery electric vehicles and gasoline vehicles subject to battery swapping stations and road grade constraints. Transport Res Part B Methodol 99:138–166
Yang H, Yagar S (1994) Traffic assignment and traffic control in general freeway-arterial corridor systems. Transport Res Part B Methodol 28(6):463–486
Zahedi R, Ghodusinejad MH, Aslani A et al (2022) Modelling community-scale renewable energy and electric vehicle management for cold-climate regions using machine learning. Energ Strat Rev 43:100930
Zhang R, Horesh N, Kontou E et al (2023) Electric vehicle community charging hubs in multi-unit dwellings: Scheduling and techno-economic assessment. Transp Res Part D: Transp Environ 120:103776
Zhang Y, Fan Y (2025) Equity evaluation of community-based public EV charging services - A case study of the Sacramento region. Energy Policy 198:114495
Zhou XS, Cheng Q, Wu X et al (2022) A meso-to-macro cross-resolution performance approach for connecting polynomial arrival queue model to volume-delay function with inflow demand-to-capacity ratio. Multimodal Transport 1(2):100017

Publisher's Note Springer Nature remains neutral with regard to jurisdictional claims in published maps and institutional affiliations.

Authors and Affiliations

Yang Song[1] · Xianbiao Hu[2] · Peiheng Li[3] · Xuesong Zhou[4]

✉ Xianbiao Hu
xbhu@psu.edu

Yang Song
songy2@alfredstate.edu

Peiheng Li
peheng.li2@nscorp.com

Xuesong Zhou(Simon)
xzhou74@asu.edu

[1] Civil Engineering Technology, Alfred State College, State University of New York, 10 Upper College Drive, Alfred, NY 14802, USA

[2] Department of Civil and Environmental Engineering, The Pennsylvania State University, University Park, PA, USA

[3] Norfolk Southern Corporation, 650 W Peachtree St NE, Atlanta, GA 30308, USA

[4] School of Sustainable Engineering and the Built Environment, Arizona State University, Tempe, AZ, USA